 doi:10.20944/preprints202102.0121.v1

Article

Multiscale Assessment of Caprock Integrity for Geologic Carbon Storage in the Pennsylvanian Farnsworth Unit, Texas, USA

Natasha Trujillo[1], Dylan Rose-Coss[2], Jason E. Heath[3,*], Thomas A Dewers[4], William Ampomah[5], Peter S. Mozley[6], and Martha Cather[7]

[1] New Mexico Institute of Mining and Technology, Earth and Environmental Science Department, Socorro New Mexico; Present Affiliation: Pioneer Natural Resources Company, Midland Texas, USA; ntrujill5@gmail.com;
[2] New Mexico Institute of Mining and Technology, Earth and Environmental Science Department, Socorro New Mexico Present Affiliation: New Mexico State Oil Conservation Division, Santa Fe, New Mexico, USA; dylan435@gmail.com;
[3] Sandia National Laboratories, Geomechanics Department, Albuquerque, New Mexico, USA; jeheath@sandia.gov
[4] Sandia National Laboratories, Nuclear Waste Disposal Research and Analysis, Albuquerque, New Mexico, USA; tdewers@sandia.gov
[5] New Mexico Institute of Mining and Technology, Petroleum Resource Recovery Center, Socorro, New Mexico, USA; William.Ampomah@nmt.edu
[6] New Mexico Institute of Mining and Technology, Associate Vice President for Academic Affairs and Earth and Environmental Science Department, Socorro, New Mexico; Peter.Mozley@nmt.edu
[7] New Mexico Institute of Mining and Technology, Petroleum Resource Recovery Center, Socorro New Mexico; Martha.Cather@nmt.edu
* Correspondence: jeheath@sandia.gov; Tel: +1-505-845-1375 (J.E.H.)

Abstract: The assessment of caprock integrity for underground storage of CO_2 and/or enhanced oil recovery (EOR) systems is a multiscale endeavor. Caprock sealing behavior depends on coupled processes that operate over a broad range of length and time scales including nanoscale heterogeneity in capillary and wettability properties to depositional heterogeneity that is basin wide. Larger-scale sedimentary architecture, fractures, and faults can govern properties of potential "seal-bypass" systems that may be difficult to assess. We present a multiscale investigation of geologic sealing integrity of the caprock system that overlies the Morrow B sandstone reservoir, Farnsworth Unit, Texas, USA. The Morrow B sandstone is the target geologic unit for an on-going combined CO_2 storage–EOR project by the Southwest Regional Partnership on Carbon Sequestration (SWP). Methods and/or data encompass small-to-large scales, including: petrography using electron and optical microscopy; mercury porosimetry; core examinations of sedimentary architecture and fractures; well logs; a suite of geomechanical testing; and a noble gas profile through sealing lithologies into the reservoir, as preserved from fresh core. The combined data set allows a comprehensive examination of sealing quality by scale, by primary features that control sealing behavior, and an assessment of sealing behavior over geologic time.

Keywords: carbon sequestration; caprock integrity; noble gas migration; seal by-pass

1. Introduction

Preprints (www.preprints.org) | NOT PEER-REVIEWED | Posted: 3 February 2021 doi:10.20944/preprints202102.0121.v1

The Site Characterization program of the Southwest Regional Partnership on Carbon Sequestration (SWP) is assessing integrity of caprock formations that immediately overlie the Pennsylvanian Morrow B sandstone, which is the target reservoir for a combined carbon capture, utilization, and storage (CCUS) project involving enhanced subsurface oil recovery (EOR)–CO_2 storage at the Farnsworth Unit (FWU), Texas, USA. Caprock integrity is the ability of generally low permeability and high capillary entry pressure formations overlying a reservoir—typically referred to as caprocks or seals—to impede movement of fluids from the reservoir below. Capillary sealing behavior arises from the nanoscale pore throats and interfacial fluid properties of the wetting phase in the caprock (e.g., brine) and the non-wetting phase of the reservoir (e.g., CO_2 or hydrocarbons). However, caprocks may contain "seal-bypass systems", which are features and/or processes that allows reservoir fluids to move out of the reservoir [1] and wettability of reservoir and caprock can be altered by carbon storage and/or enhanced hydrocarbon recovery procedures [2]. Seal-bypass systems may include discontinuous coverage of the sealing lithologies over the reservoir, natural or induced fracture networks, faults, permeable injectites (i.e., structures formed by sediment injection) or other geologic pipe structures, and man-made intrusions such as leaky wellbores [1]. Implicit in the concept of caprock sealing behavior is a timescale of interest, which for geologic CO_2 storage is 100s to 1000s of years.

This chapter presents a caprock integrity study that focuses on evaluating geologic sealing behavior for capillary, fluid flow, and mechanical properties at different spatial and temporal scales. Specifically, we assess: 1. pore-scale capillary sealing and microstructure; 2. Local seal bypass mechanisms; 3. Seal regional lateral continuity across reservoir scales; and 4. Mechanical integrity of the reservoir-caprock package to fluid pressure perturbation. This requires a multi-scale approach using a variety of techniques to cover the range of length scales, processes, and features involved in caprock integrity (Figure 1). To these ends we examine sub-core scale capillary heterogeneity of the reservoir and sealing lithologies of the Morrow-B sandstone lithologies, the upper Morrow shale top seal, and the overlying Thirteen Finger Limestone secondary sealing lithologies using mercury porosimetry. We examine evidence for existing fractures and faults that could serve as seal bypass systems under present day stress orientations, as well as examining geomechanical constraints on induced seal bypass features associated with CCUS and EOR activities within the FWU. The lateral continuity of sealing units in the Farnsworth is assessed via subsurface mapping. The large-scale sealing capacity of these lithologies as have occurred over geologic time is assessed using noble gas measurements collected from fresh core. Formation-scale features examining the scale of the entire Farnsworth Unit and regional stratigraphic architecture using seismic methods have been discussed by Rose Coss et al. [3, 4] and Ampomah et al. [5].

Preprints (www.preprints.org) | NOT PEER-REVIEWED | Posted: 3 February 2021 doi:10.20944/preprints202102.0121.v1

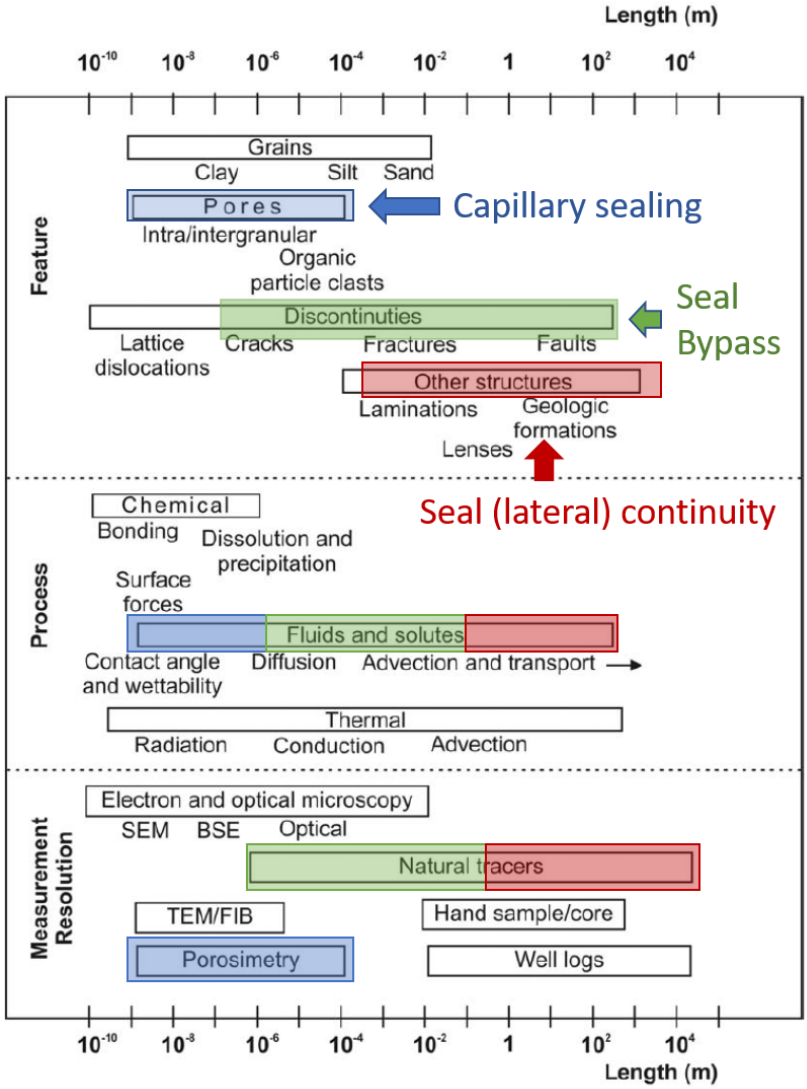

Figure 1. Features, processes, and measurement resolution relevant to assessment of caprock integrity (adapted from DOE [6] and Heath [7]).

2. Site Location and Geologic Setting

2.1 Unit History and General Geology

The Farnsworth Unit (FWU) is located in Ochiltree county, Texas, USA (Figure 2), with nearby Arkalon Ethanol Plant and Agrium Fertilizer Plant supplying anthropogenic CO_2 for enhanced oil recovery in the field. Production and injection at FWU occur strictly within the Pennsylvanian Morrow B sandstone (Figure 3; [5]). "Morrow" is an operational name that refers to a sequence of alternating mudstone and sandstone intervals deposited during the Morrowan period of the late Pennsylvanian [8]. The Morrow B delineates the first sandstone package deposited below the Atokan Thirteen Finger Limestone [9,10].

The primary caprock intervals at FWU are comprised of the upper Morrow shale and the Thirteen Finger Limestone (Figure 3). The Thirteen Finger Limestone is another informal name for a series of predominantly carbonate cementstone intervals that are intercalated with a

Preprints (www.preprints.org) | NOT PEER-REVIEWED | Posted: 3 February 2021 doi:10.20944/preprints202102.0121.v1

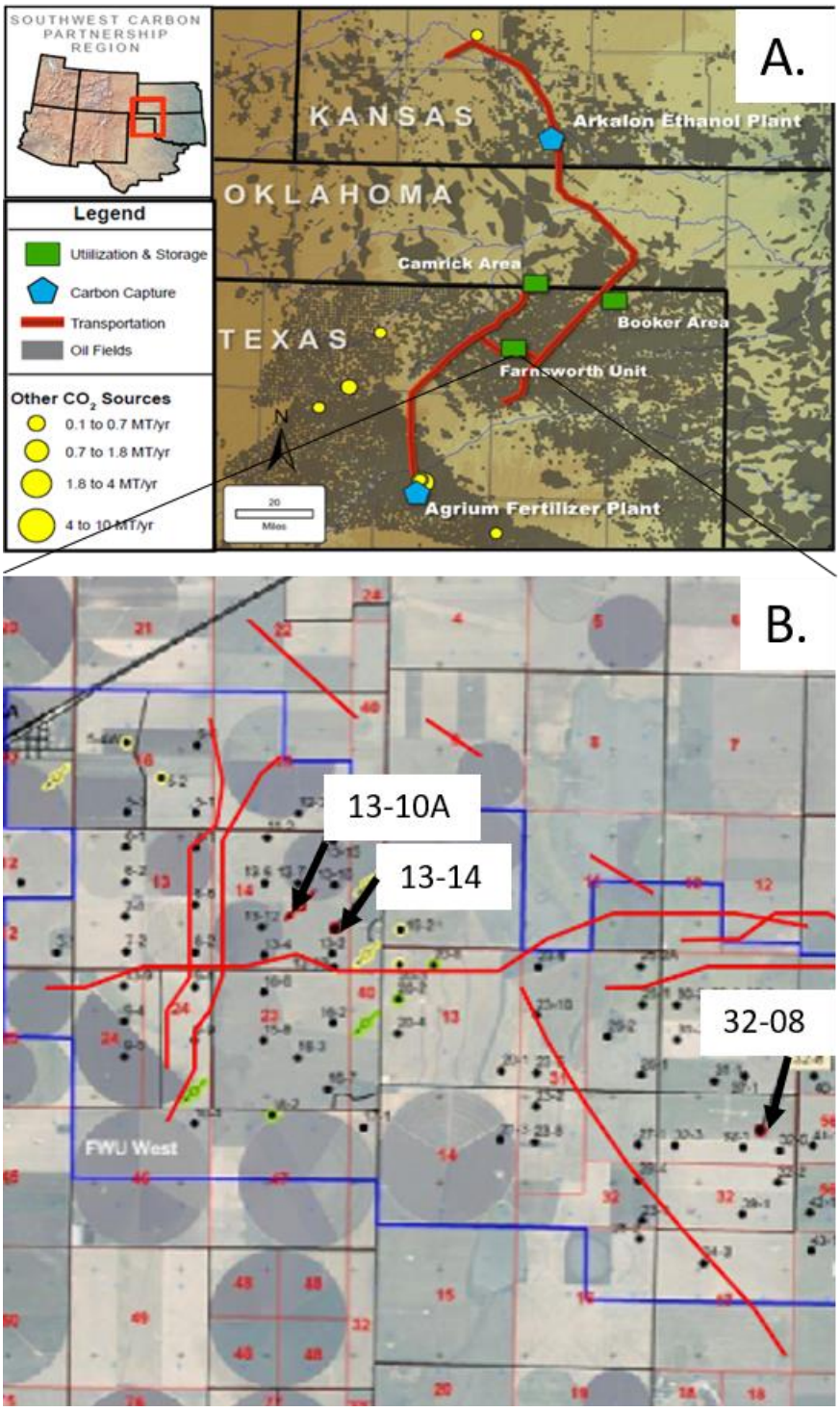

Figure 2. A. Upper left, SWP region map. Lower left, legend used in field location map (right). Location of oil fields undergoing enhance oil recovery utilizing anthropogenic CO_2. CO_2 is piped (red lines) from the Arkalon Ethanol plant in Liberal Kansas, USA and the Agrium Fertilizer facility of Borger Texas, USA. Modified from Balch and McPherson [11]. B. Locations of wells in the Farnsworth Unit (outlined in blue) used in assessing local and field-wide caprock integrity. Red lines in (B) show locations of inferred faults (modified from Hutton, [12]).

black carbonaceous mudstone that were deposited during the Atokan period of the late Pennsylvanian (Figure 3; see also Trujillo [8], and Rose-Coss, [7]). Both the Morrowan and Atokan intervals are common throughout the Texas and Oklahoma panhandles, southeastern Colorado, and western Kansas. Overlying stratigraphy includes Late Pennsylvanian through the Middle Permian shales and limestones, with lesser amounts of dolomite, sandstone and evaporites [7, 12-14]

Preprints (www.preprints.org) | NOT PEER-REVIEWED | Posted: 3 February 2021 doi:10.20944/preprints202102.0121.v1

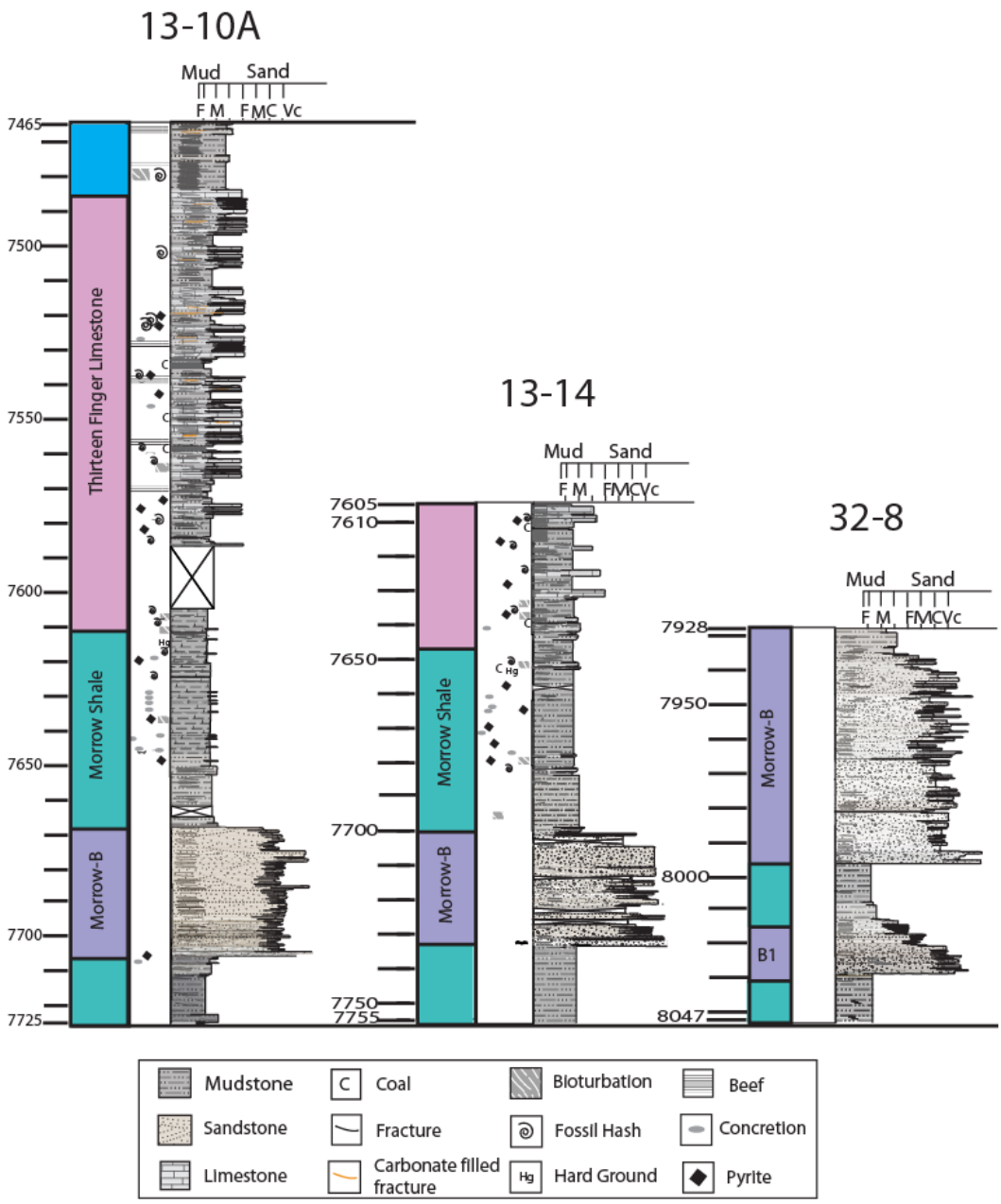

Figure 3. Stratigraphic columns of three SWP characterization wells (from Rose-Coss[9]; expanded versions found in his Appendix B).

2.2 Tectonic Setting

The FWU sits on the northwest shelf of the Anadarko basin in the Texas Panhandle. From the FWU, the basin plunges to the southeast where it reaches depths of over 40,000 ft (12,192 m) adjacent to the Amarillo-Wichita Uplift [15, 16]. Maximum rates of subsidence occurred during Morrowan to Atokan times [14-17]. Positive features which might have influenced deposition within the region include the Ancestral Rockies to the north, the Central Kansas uplift to the north-east, and the Wichita-Amarillo uplift to the south [17,18]. The structural grain of the basin was inherited from the Precambrian to Cambrian failed arm of a triple junction known as the Southern Oklahoma Aulacogen [15,16]. The region was then tectonically quiet until the beginning of the Chesterian-Morrowan, when the Wichita-Amarillo uplift and the ancestral Rockies formed as a result of northeast-directed

Preprints (www.preprints.org) | NOT PEER-REVIEWED | Posted: 3 February 2021 doi:10.20944/preprints202102.0121.v1

basement-involved thrust faulting associated with collision between the North American and Gondwanan plates [14,15,19,20]. Fault movement within the Wichita-Amarillo uplift is characterized by vertical block movement and left-lateral strike slip movement. The vertical fault movement occurred began in the Chesterian and then continued predominantly at the end of the Morrowan into the Atokan time period [17]. This period of faulting created normal faults with a down to the south displacement parallel to the axis of shear associated with the Amarillo uplift. The left lateral strike slip movement occurred afterwards in the late-to-post Atokan and is expressed as anticlinal horst blocks and synformal grabens diverging at intersections from the main shear zones [17]. Tectonic activity slowed after the Atokan and the region was quiescent by the end of the Pennsylvanian. Local uplifts and associated basins combined with climate variations at time of deposition set the stage for the stratigraphic variations seen in core, and especially evident in the Thirteen Finger Limestone, discussed below.

3. Materials and Methods

3.1 Coring Program, Petrologic Description, and Well Log Analysis

The coring program was designed and implemented in 2013 and 2014 by the SWP and former operator Chaparral Energy LLC, which targeted the primary Morrow B sandstone reservoir and the overlying caprocks, the upper Morrow shale and the Thirteen Finger Limestone. A review of core collected by previous developers of the FWU was conducted by the SWP at the CGG core warehouse in Schluenburg, Texas, during this time, which resulted in production of stratigraphic columns for planning of SWP characterization wells. Locations of the resulting three cored wells were chosen to enable comparison of reservoir properties of the west and east sides of the Farnsworth Unit. The coring program included core analysis plans to support major SWP project objectives and/or research topics on CO_2 storage capacity, injectivity, and plume extent; storage permanence; and injection- and/or production-induced reservoir damage. Thus, the planning encompassed a suite of testing, including petrophysics, petrology, geomechanics, and geochemistry.

Schlumberger ran a large suite of wire-line tools for caprock and reservoir characterization, and wellbore integrity assessment in cooperation with the SWP, which had personnel in the field to observe drilling and coring of Well 13-10A and Well 13-14, and to assist with core preservation and core handling. Terra Tek, a former Schlumberger company, performed core handling in the field and initially housed the core for initial core characterization and sampling. Several pieces of fresh core from well 13-10A were sampled and preserved in the field immediately after core retrieval to the Earth's surface for noble gas analysis. Initial core reviews were performed by Sandia National Laboratories (SNL), New Mexico Tech (NMT), and Chaparral Energy to choose sample locations for petrologic, petrophysical, geomechanical, and geochemical analysis to be performed by Terra Tek, SNL, and NMT. SNL and NMT coauthors submitted formal sampling and analysis plans to Terra Tek, which included sampling and/or analysis for thin sections (of the caprocks and reservoir rocks and of fractures), relative permeability and capillary pressure, routine plug analysis, mercury porosimetry, Routine Core Plug (RCPA) and Tight Rock Analysis (TRA) (both by Terra Tek), X-ray diffraction, geochemical analyses including pyrolysis and vitrinite reflectance, and geomechanical testing. To help quantify heterogeneity and guide sampling densities for laboratory testing, the multi-

Preprints (www.preprints.org) | NOT PEER-REVIEWED | Posted: 3 February 2021 doi:10.20944/preprints202102.0121.v1

well Heterogeneous Rock Analysis (HRA; [21]) was performed by Schlumberger. For HRA of FWU reservoir and caprock lithologies, results of gamma ray, deep resistivity, bulk density, neutron porosity, and compressional slowness logs were combined with caliper responses to make a preliminary assessment of rock classes, which resulted in determining eleven separate rock unit classes: two for the reservoir lithology (Morrow-B) and nine for the caprock lithologies (upper and lower Morrow shale and Thirteen Finger Limestone). The results of these analyses are included in our assessment of caprock integrity as discussed below. More discussion on core descriptions and core photographs are found in Rose-Coss et al. [9] and Trujillo et al. [10].

3.2 Petrologic Characterization

Petrologic methods involve standard thin section petrography and backscattered electron microscopy conducted at both SNL and NMT. Twelve thin sections were half-coated with carbon from well 13-10A for electron microprobe analysis, with the remaining half uncoated to allow for other analyses. The thin sections were analyzed using a Cameca SX-100 microprobe that has three wavelength dispersive spectrometers along with secondary electron and high-speed backscattered electron detectors. The beam diameter was 20 μm and 10 μm for clay minerals. These thin sections were analyzed at the New Mexico Bureau of Geology and Mineral Resources (NMBGMR) at NMT. Backscattered electron (BSE) images were taken to help determine mineral composition and phases. The images were taken and analyzed in a preliminary manner by Lynne Heizler of NMBGMR, who identified the mineral phases. The backscattered electron images were correlated with the optical thin section photomicrographs to determine mineral composition especially for the carbonate and clay minerals. The BSE images helped constrain the diagenetic history by determining any mineral alteration of different phase compositions.

3.3 Petrophysics

3.3.1 Retort Analysis

Retort oil and water saturation measurements were performed on core (biscuit) samples by Terra Tek. Porosity, grain density, and fluid saturation were calculated from a representative portion of the crushed sample, and the whole sample was used for bulk density determination. The total weight and bulk volume were determined for each sample, and then the sample was crushed and sieved until a significant portion of the sample was of the proper size range. The crushed sample was then weighed and placed in a retort vessel and heated to an initial temperature stage to collect the interstitial water. Once the production of fluid had ceased, the temperature of the retort vessel was elevated to remove all remaining condensate and light mobile hydrocarbons. Finally, the temperature was elevated to the final stage to remove any remaining fluids including bound water and any interstitial oil, or 'cracked' kerogen hydrocarbons. The sieved sample, prior to retorting was weighed and the partial grain volume (grain volume plus interstitial fluid volume) of each sample was determined by Boyle's Law technique in order to measure the gas-filled pore space (BV-GV partial). The porosity, bulk density, grain density, and fluid saturation were then calculated.

3.3.2 Pulse Decay Permeability Analysis

Pulse-decay permeability was measured on core plug samples by Terra Tek at 'as received' saturation conditions. If microfractures were present, the plugs were first prepared by injecting with

Preprints (www.preprints.org) | NOT PEER-REVIEWED | Posted: 3 February 2021 doi:10.20944/preprints202102.0121.v1

a penetrating epoxy resin to fill the stress-release microfractures. The sample ends were then trimmed, and pre-weighed 18-mesh screens were added for gas distribution over the end faces of the sample. Each sample was then placed in a hydrostatic core holder and allowed to reach net overburden and pore pressure equilibrium. Sample permeability was then measured by the pulse-decay method.

3.3.3 Pressure Decay Permeability for Tight Rock Analysis (TRA)

Pressure Decay Permeability was measured on samples at 'as received' saturation conditions (measured prior to additional processing). A specific weight fraction of crushed, sieved sample material was loaded into a matrix cup for gas expansion. Data derived from the gas expansion measurement was used to calculate the permeability to gas. Because the sample was crushed, the permeability measurement was not conducted at net overburden conditions; however, a proprietary correlation for net overburden data has been developed and routinely used for specific shale types and was applied to analysis of rock samples herein.

3.3.4 Mercury Porosimetry

Intrusion-extrusion mercury porosimetry was performed on core plugs by Poro-Technology, a Micromeritics company, using a Micromeritics AutoPore IV 9500 Series porosimeter. Core plugs were oriented either vertically or horizontally (i.e., parallel or perpendicular to the long axis of the core). The core plugs were approximately 0.9-inch (2.3 cm) diameter by 0.9-inch (2.3 cm) long and were jacketed with epoxy for directional intrusion. Poro-Technology made closure corrections accounting for volumes of mercury injected that did not penetrate into the pore space prior to the pressure achieving the mercury entry pressure of the pore space. Breakthrough pressure, or the pressure at which a non-wetting phase penetrates a rock through the connected pore space [22], was estimated for core plugs using methods of Dewhurst et al. [23]. Breakthrough pressures were converted from the mercury-air system to a CO_2-water system and to CO_2 column heights using the methods of Ingram et al. [24]. We use an interfacial tension value of 484 mN/m for mercury-air-rock system, and a contact angle of 140°. We assumed a geothermal gradient of 25°C/km and a hydrostatic pressure gradient of 0.0098 MPa/m to estimate the density of CO_2 and water at the depths of the core plugs. Interfacial tension values for the water-CO_2 system assumed zero ionic strength and used the methods of Heath et al. [25]. Contact angles for the water-CO_2-mineral system were estimated from Iglauer et al. [26] for quartz, calcite, and mica, resulting in a range of 10^{o} to 57°.

3.4 Geomechanics Analysis

A series of rock mechanical tests were performed on rock core sampled and tested at Terra Tek's laboratories in Salt Lake City, Utah, using standard techniques. These include Brazil tension (or cylinder splitting) tests, unconfined compression tests, and triaxial compression tests. These were used to extract static elastic properties, rock unconfined and triaxial strength, and tensile strength information from samples from all three SWP characterization wells in the FWU. A standard Mohr-circle analysis was used to delineate failure envelopes for sampled lithologies.

3.5 Fracture Analysis

Under the guidance of the SNL and NMT coauthors, Terra Tek performed detailed analysis of macroscope fractures on nearly 270 ft of continuous whole core from Well 13-10A. The fracture

Preprints (www.preprints.org) | NOT PEER-REVIEWED | Posted: 3 February 2021 doi:10.20944/preprints202102.0121.v1

descriptions focused on identifying fracture types based on morphologic characteristics and intensity. As the core was not oriented, Terra Tek drew an arbitrary "North" line on the core to enable measurement of relative orientation of measured fractures. Fracture attributes measured include fracture strike and dip, general fracture type, type of mineral fill, type of oil stain, fracture porosity, fracture spacing, and intensity of fractures for each cored interval. Fracture classes include those induced from drilling or coring versus natural fractures that may or may not exhibit shear, extension, or mineralization. Terra Tek analysis included tabulation of fracture types by depth and stereo plots of relative fracture orientations by fracture type.

3.6 Preservation of Fresh Core and Noble Gas Analysis

Core preservation for noble and other pore fluid gases followed procedures found in Osenbrück [27]. Specially designed canisters were built from high-vacuum service equipment to seal samples against atmospheric contamination or significant pore fluid degassing. Core was preserved immediately in the field after the core was retrieved to Earth's surface and slabbed in the field to obtain samples. After sub-sampling of core from Well 13-10A, samples were weighed and sealed in canisters. A purging and vacuum pump-down process evacuated atmospheric noble gases from the canisters. Helium, neon, and argon isotopes were analyzed at the University of Utah's Dissolved and Noble Gas Laboratory in Salt Lake City, Utah, USA. After transfer of the gases into a purification line, analysis followed methods described by Hendry et al. [28] using quadrupole and magnetic sector field mass spectrometers.

4. Results

As stated in the introduction, caprock integrity for EOR-CCUS is a multiscale assessment of the ability of a caprock lithology or set of lithologies to sustain emplacement of a body of CO_2 for a given time. For CCUS, this may be 100s or 1000s of years. One aspect for CCUS which is favorable for use of CO_2 for oil recovery and storage is the fact that the same caprock invoked for CO_2 uses is the same caprock involved in oil and gas storage over geologic time. We know from the long history of subsurface engineering at FWU that storage under EOR conditions is favorable for CO_2 containment. We need to build confidence that injection and emplacement conditions under CCUS best practices does nothing to threaten the integrity of caprock lithologies. To this end, we examine integrity of the FWU upper Morrow shale and Thirteen Finger Limestone from three perspectives: 1. The ability of the intact lithologies to sustain a capillary seal to CO_2 of a given volume or column height; 2. The nature of existing fractures and faults to serve as seal bypass features, as well as assessing potential for creation of new fractures or reactivating old ones under injection-perturbed stress conditions; and 3. The physical, stratigraphic continuity and consistency/heterogeneity in the caprock lithologies over the reservoir extent. We address each of these in turn, and then turn to noble gas distributions over the reservoir-caprock package in an integrated method for addressing caprock integrity over the scales of interest.

Preprints (www.preprints.org) | NOT PEER-REVIEWED | Posted: 3 February 2021 doi:10.20944/preprints202102.0121.v1

4.1 Primary and Secondary Caprock Sealing Behavior and CO_2 Column Heights

4.1.1 Lithofacies Interpretations of Caprock Lithologies

Figure 3 shows stratigraphic columns of each core obtained from the three characterization wells at Farnsworth (the 13-10A, 13-14, and 32-8), depicting the extent of mud and sand in the clastic mixture, including fractured zones, depositional fabrics (i.e., carbonate hardgrounds, burrows, and coal cleats) and diagenetic features (i.e., carbonate "beef", concretions, and mineralized fractures) that could exert positive or negative influences on caprock integrity. Details about these features are found in [9] and [10].

The upper Morrow shale is a marine mudstone that directly overlies the Morrow B sandstone reservoir (Figure 3) and thus serves as the primary caprock. It is composed of three common mudstone lithofacies (Table 1) including black laminated mudstone (blM), calcareous mudstone

Table 1. FWU caprock lithofacies descriptions (after Rose-Coss, 2017), TOC analysis, and assigned color for HRA rock classification (Terra Tek).

Facies and Description	Sedimentary Features	TOC%	HRA Color
Thirteen Fingers Limestone			
(cC) Carbonate cementstone, micritic dolomite and dedolomite, grey to white	Well indurated, smooth, sparse cemented fractures, abrupt to gradational bounding surfaces	2.3	Light Blue
(bcM-a) Well indurated black carbonaceous mudstone and siltstone, locally calcareous	pyrite nodules, fossil hash, bioturbation, bedding-parallel fibrous calcite veins ("beef" of Cobold, 2013)	0.44 - 10.7	**Black**
(bcM-b) Fairly well indurated carbonaceous black mudstone	Floating sand grains, abundant to moderate burrowing	0.44 - 10.7	Purple
(bcM-c) Black mudstone and coal	Coal with thin layers of mudstone	0.44 - 10.7	Olive
(bcM-d) Black to grey laminated mudstone with silt partings	Locally dolomitic, fossiliferous, organic rich partings (plant fragments)	0.44 - 10.7	Orange
(bcM-e) Poorly indurated black carbonaceous mudstone	Locally dolomitic, fossiliferous	0.44 - 10.7	Grey
Morrow shale			
(cM) Calcareous mudstone, brown to grey, green laminated to massive, broken and bioturbated sections, friable	Slightly fossiliferous, laminations, bioturbation, coal	0.44-10.7	Brown
(blM) Black, laminated mudstone	Low angle to planar laminations, concretions, fossil hash	0.53 - 2.7	Red
(gbM) Friable, bioturbated mudstone, olive to gray, laminated to massive, friable	Low angle to planar weak laminations, low to moderate bioturbation, abundant microfossils	0.30-1.0	Yellow

(cM) and green bioturbated mudstone (gbM) as determined [9]. The lower portions of the upper Morrow shale consist of the gbM facies, which is transitional from the sands of the Morrow B reservoir. The green bioturbated mudstone (gbM) lithology is a slightly fossiliferous, organic-rich, slightly calcareous mudstone, that contains scattered quartz, feldspar, muscovite, and calcareous fossil-hash silt. The middle portion of the upper Morrow shale consists of the blM facies, which is interpreted by [9] to be deposited under anoxic conditions, consisting of fissile, slightly fossiliferous organic-rich mudstone. This facies gradually transitions upward into the cM facies, a more friable and calcareous mudstone that contains several hardgrounds (i.e., cemented paleo sea-floor surfaces) that are found to be laterally continuous through the FWU [9,10]. The variable degree of cementation in the cM facies imparts a heterogeneity to the geomechanical response, as discussed later.

Preprints (www.preprints.org) | NOT PEER-REVIEWED | Posted: 3 February 2021 doi:10.20944/preprints202102.0121.v1

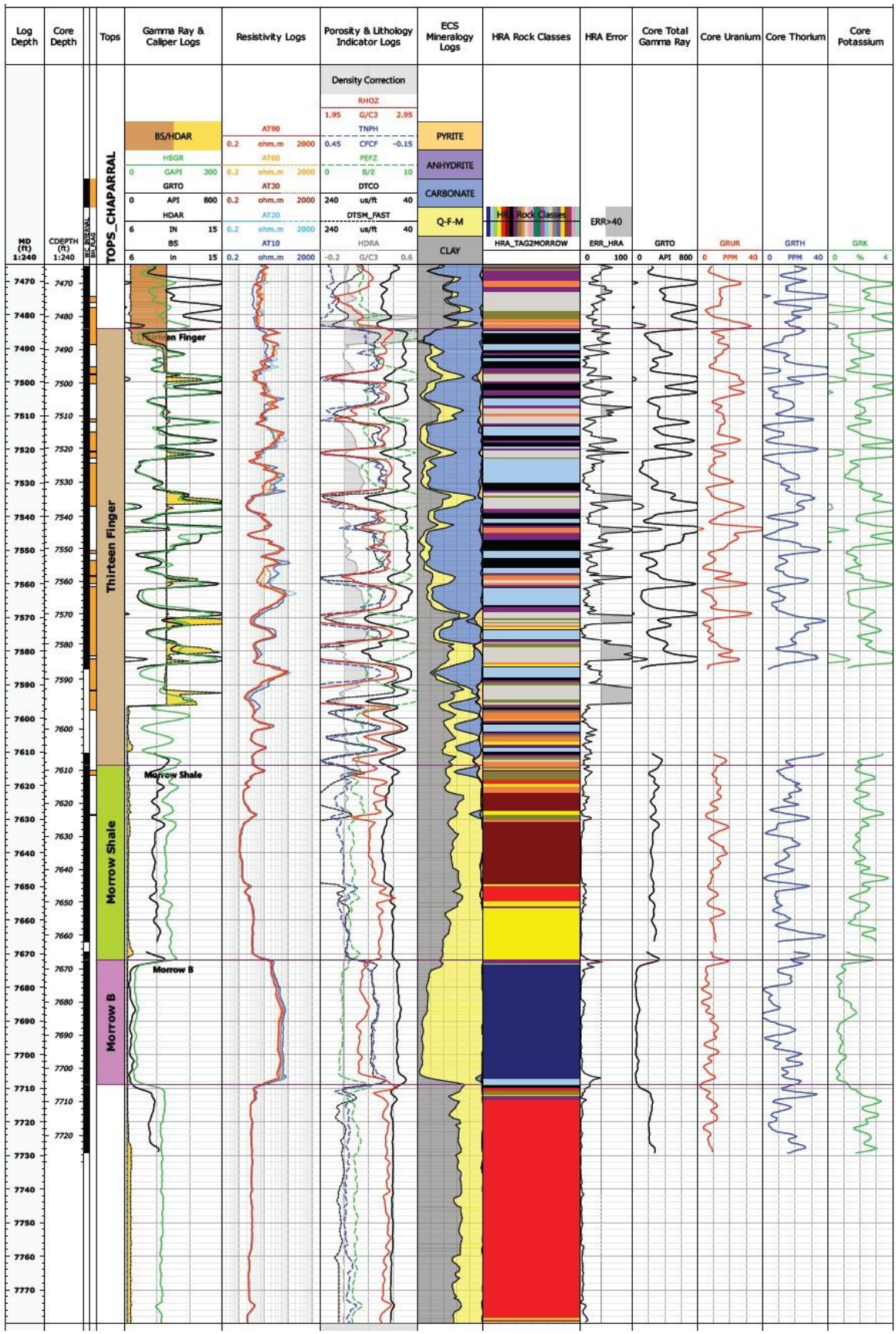

Figure 4. Well 13-10A Heterogeneous Rock Analysis Log showing color by rock unit and depth. Depths are given in feet and converted to meters by multiplying by 0.3022. Note that logging depth and coring depth contain discrepancies associated with the coring procedures.

Preprints (www.preprints.org) | NOT PEER-REVIEWED | Posted: 3 February 2021 doi:10.20944/preprints202102.0121.v1

The overlying Thirteen Finger Limestone was deposited in a marine environment that underwent several cycles of transgression and regression during deposition [29] and consists mostly of black carbonaceous mudstone (bcM) lithofacies alternating with limestone layers [9,10]. On inspection the limestone layers consist of diagenetic carbonate cement or diagenetically enhanced carbonate content and so are denoted as cementstone lithofacies (cC; references 9 and 10). Fossil hash concentrations and pyrite nodules occur in varying amounts throughout the mudstone lithology, and there are some coal seams of varying thickness. The Thirteen Finger Limestone is a widely distributed formation with a distinct wireline log signature with recognized open and healed vertical fractures that may provide a permeable network [30].

The caprock lithofacies in Table 1 are mapped onto the Terra Tek HRA classification scheme denoted by the color scheme in the last column of Table 1. Note that the Terra Tek HRA procedure recognizes variability in the mechanical integrity of the bcM lithofacies of the Thirteen Finger Limestone, and we have denoted this by additional labels (i.e. bcM-a, bcM-b, etc.). Figure 4 summarizes results of the HRA performed by Terra Tek from well log variability in the 13-10A well. The HRA facies designations are shown by the color strip down the middle of the figure, and one can discern the Morrow B sandstone (dark blue), lower Morrow shale (red), upper Morrow shale (yellow, red, and brown going from deeper to shallower), and the Thirteen Fingers Limestone, with multiple alternating bands of color. The lithology breaks in the Thirteen Finger Limestone are easily discernable from gamma and density logs; for example, close examination of the density logs and gamma ray "kicks" reveals the storied thirteen shale members of the Thirteen Fingers Limestone alternating with the carbonate layers (designated by the light blue color bands). Variability in the mechanical integrity within the shale layers of the Thirteen Finger Limestone is manifest in five distinguishable subunits of the bcM lithology, shown by separate colors. Later we distinguish these layers in terms of mechanical behavior, and, for example, moving from elastically stiff to compliant layers we would have the HRA color designations Black > Purple > Olive > Orange > Grey. HRA logs for wells 13-14 and 32-8 are given by Figures SM1 and SM2 in the Supplemental Material accompanying this paper. The HRA analysis is most commonly performed in the realm of unconventional "shale" reservoirs [21; 31-33] and is a means to better understand mudstone lithological variability given the poor core recovery and general difficulty in obtaining core-plug samples for standard analyses, which can lead to a sampling bias and over-representation of the strengths of these materials.

A mapping of HRA color designations and facies designations from core logging performed by Rose-Coss [9] is facilitated by petrographic observations from thin sections prepared from core obtained from the 13-10A, 13-14, and 32-8 wells. These were performed by Steve Cather of the NMBGMR (Personal Communication, 2017) and are summarized in Tables SM-1, -2, and -3 in the Supplemental Material. From this, we determine that the Orange HRA refers to Bcm facies with more abundant carbonate, the Olive designation refers to coal layers and the black mudstone above and below that encapsulates them, and the grey Bcm lithofacies is the least indurated, and as such has the least dynamic and static elastic moduli (shown later). Black and Purple HRA units are the most indurated of the bcM facies.

The caprock lithologies would classify as silt- (quartz, carbonate, organic matter) bearing clay-rich mudstone and clay-dominated mudstone (Figure 5A and B; classification of Macquaker and

Preprints (www.preprints.org) | NOT PEER-REVIEWED | Posted: 3 February 2021 doi:10.20944/preprints202102.0121.v1

Adams [34]). From thin section observation [9,10], the mudstones contain variable amounts of organic matter, quartz, and macro and microfossils. Authigenic pyrite, calcite, and dolomite are common. Many of the cementstone layers contain fractures, many of which are filled with carbonate cement [10]. The limestone is somewhat unusual, in that, at least for the few samples analyzed thus far, it is dominated by diagenetic carbonate (Figure 5C and D). The limestone locally contains significant biogenic carbonate [10]. Thus, most of the limestones in the Thirteen Finger Limestone are more properly classified as cementstones. This interpretation is supported by the obvious occurrence of concretions in the core (Figure 5D), which are similar in character to the limestone beds.

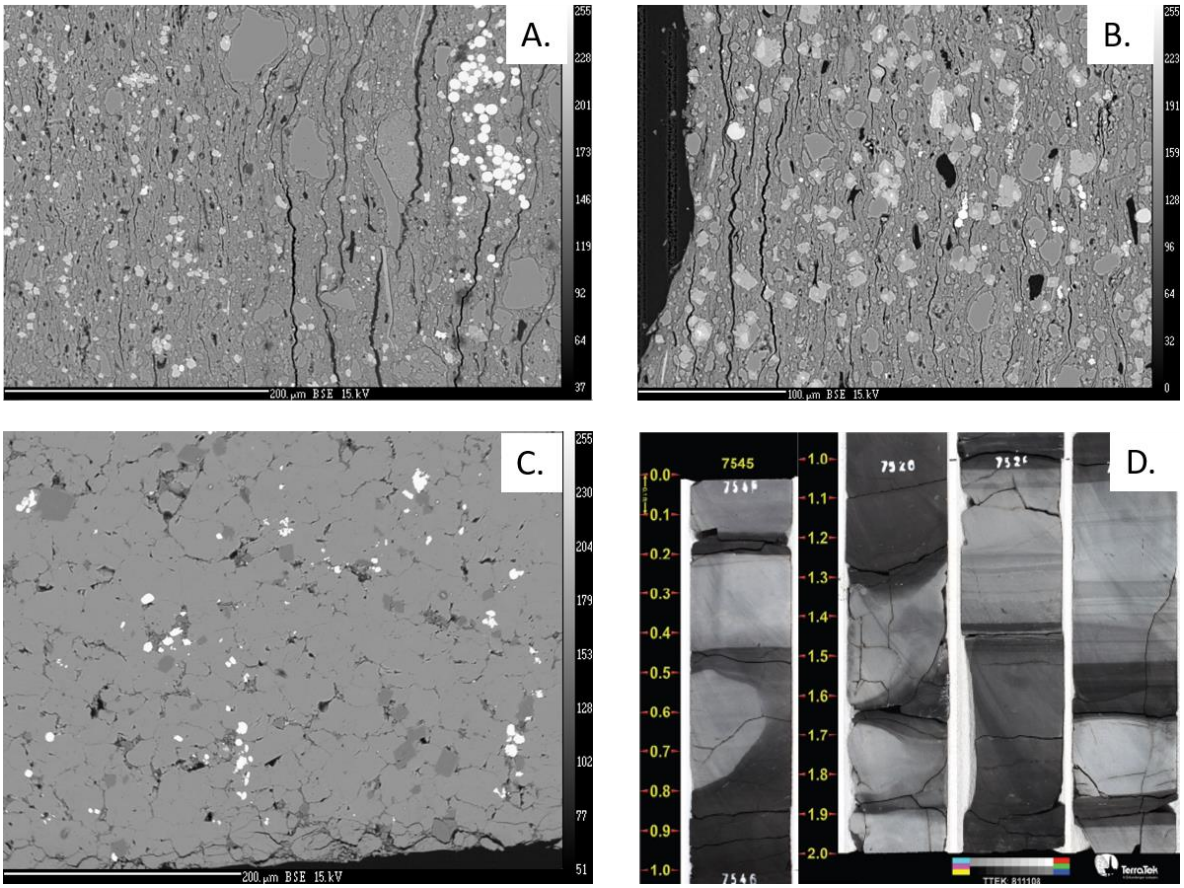

Figure 5. **A.** Back-scattered electron image of a silt (carbonate, organic matter) bearing clay-rich mudstone in the Morrow Shale. Stratigraphic-up is to the left, with siltier rich laminae on the left and clay-rich laminae on the right. Black portions are organic matter, and white features are pyrite framboids. Well 13-10a, 7633.76 ft. **B.** Backscattered electron image of silt (quartz, calcite, organic matter) bearing clay-rich mudstone in the Morrow Shale. Stratigraphic-up is to the left. Black particles are organic matter, irregular dark gray particles are quartz, light gray rhombs are ankerite, white grains are pyrite. Well 13-10a, 7632.6 ft. **C.** Backscattered electron image showing calcite (light gray), dolomite (dark gray), and pyrite (white) cemented mudstone (cementstone) in the Thirteen Fingers, Well 13-10a, 7540.65 ft. **D.** Core photographs showing variable geometry of limestones in the Thirteen Fingers Limestone. Some limestones are laterally continuous throughout the width of the core, whereas other are laterally discontinuous (concretionary). Well 13-10a, depths indicated on photo. See [9, 10]]) for additional images and descriptions.

While most of our attention is devoted to the caprock, we refer to lithologies in the Morrow B sandstone reservoir for comparison purposes. Lithologic descriptors associated with the color codes for the Morrow B sandstones are far simpler and relate to the hydrologic flow units discussed by [2] and [4], carrying a Dark Blue or Green HRA designation as shown in Figure 4 above and Figure SM-1 and SM-2 in the Supplemental Material.

4.1.2 Porosity and Permeability by Lithofacies

Preprints (www.preprints.org) | NOT PEER-REVIEWED | Posted: 3 February 2021 doi:10.20944/preprints202102.0121.v1

Porosity, water and oil saturation, and gas permeability for a range of rock types in each of the characterization wells were analyzed via Terra Tek's RCA at depth intervals of approximately three feet if core plugs were attainable, and these are mostly reservoir lithologies. Data for well 13-10A are given in the Appendix of Rasmussen et al. [2]; data for the other two wells (13-14 and 32-8) are given Table SM-4 in the Supplemental Material, color coded by HRA rock class. Data in these tables are mostly associated with the sandstone members in the Morrow B sandstone reservoir and determined from analysis of core plugs at the indicated depths.

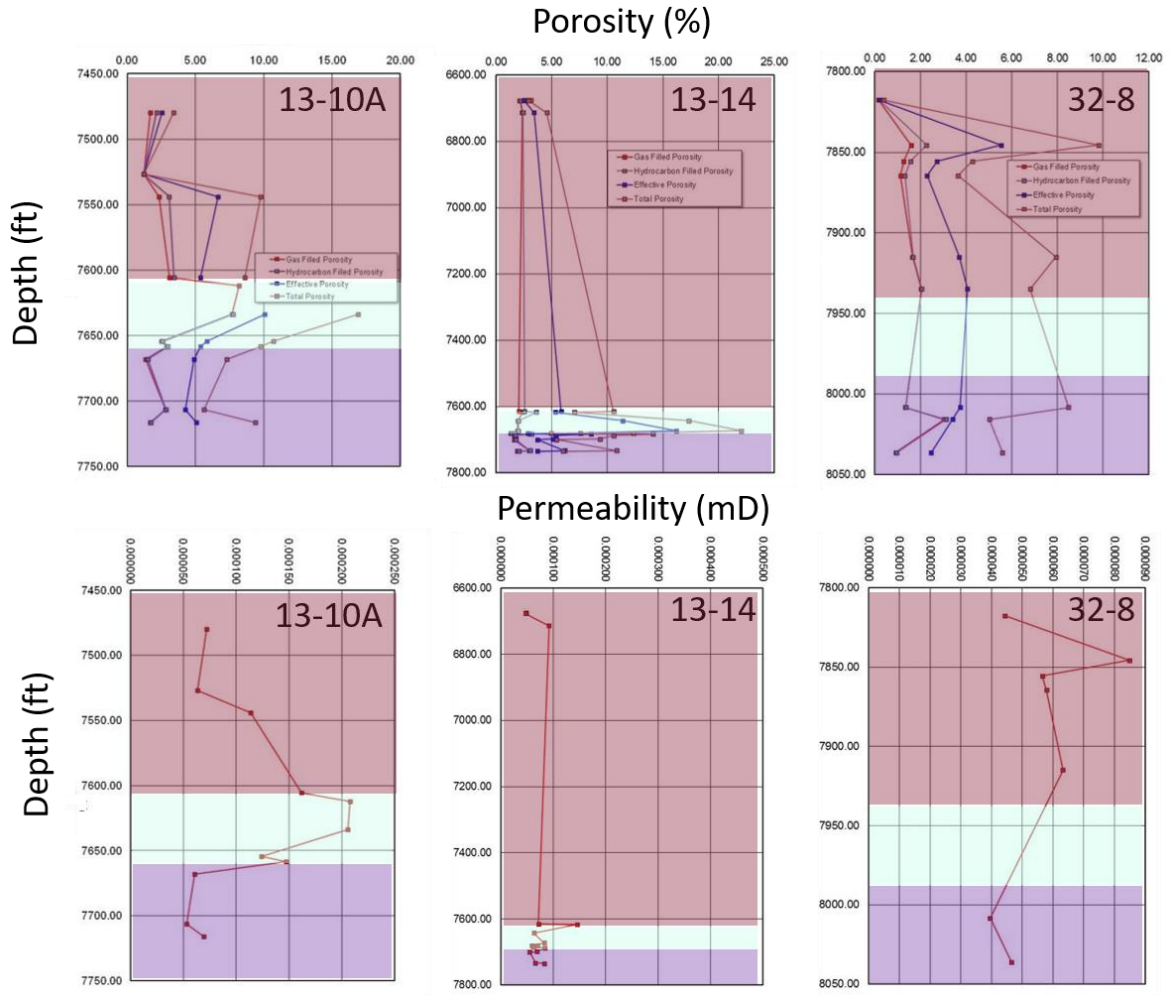

Figure 6. Porosity and permeability of Farnsworth reservoir Morrow B Sandstone (purple), and Farnsworth sealing lithologies Morrow Shale (green), and Thirteen Fingers (pink) for wells 13-10A, 13-14, and 32-8. Color schemes and depths corresponds to those in Figure 3. Data were determined from Terra Tek's Tight Rock Analysis (TRA) methodology.

The low permeabilities of mudstone and limestone members of the caprock lithologies were analyzed using a pulse decay permeability method proprietary to Terra Tek's TRA methodology. This method allows determination of gas-filled porosity, hydrocarbon filled porosity, effective gas saturation, as well as total porosity and permeability among other parameters. These results are summarized in Table SM-5 for all three characterization wells and are mapped to both the caprock facies designation of [9] and the HRA color unit. In Figure 6 we plot total porosity and permeability by depth for mudstone members of the Morrow B sandstone (depth range shown in purple),

Preprints (www.preprints.org) | NOT PEER-REVIEWED | Posted: 3 February 2021 doi:10.20944/preprints202102.0121.v1

mudstone members of the overlying upper Morrow shale (depth range shown in green), and mudstone and limestone members of the Thirteen Fingers Limestone (depth range shown in pink).

While there is well-to-well variability, in general the Morrow shale mudstones have higher porosity and slightly higher permeability than mudstone and limestone in the other formations. Porosities and permeabilities of the hydrologic flow units in the Morrow B sandstone are considerably higher, with porosity values ranging largely from 15 to 20%, and permeability ranging from 10 to 1000 mD (orders of magnitude higher than the mudstone facies of the caprock units at FWU shown in Figure 6; see Figure 2 in [2]).

4.1.3 Porosimetry and CO_2 Column Heights in Farnsworth Reservoir and Sealing Lithologies

Sealing capacity in the context of CCUS is the CO_2 column height that is retained by the capillarity of a water wet rock. Here, we estimate CO_2 column heights (using calculated pore throat diameters and breakthrough pressures) for the different reservoir and caprock lithologies using MICP analyses from core plug samples summarized in Table SM-6 in the Supplemental Materials. The pore throat size distributions for the Morrow B sandstone, upper Morrow shale, and the Thirteen Finger Limestone for the west and east side of the FWU are compared in Figure 7. The Morrow B sandstone (green curves) has a range in pore throat diameters from 0.003 to 1000 μm. The pore throat diameter at the maximum breakthrough pressure is 44.3 μm. This corresponds to breakthrough pressures ranging from 0.03 to 0.77 MPa (4.8 to 112 psi) for the sandstone reservoir. The average pore throat diameter for the Morrow B sandstone is 14 μm with a median of 7 μm. The Morrow B sandstone has a bimodal distribution in pore throat diameters, with samples having either a peak in the 0.3–4 μm range or 10–80 μm range. This distribution relates to sandstones in different wells, with the 10- 80 μm range for sandstones from wells 13-10A and 13-14, and the 0.3-4 μm range for the sandstones from well 32-08.

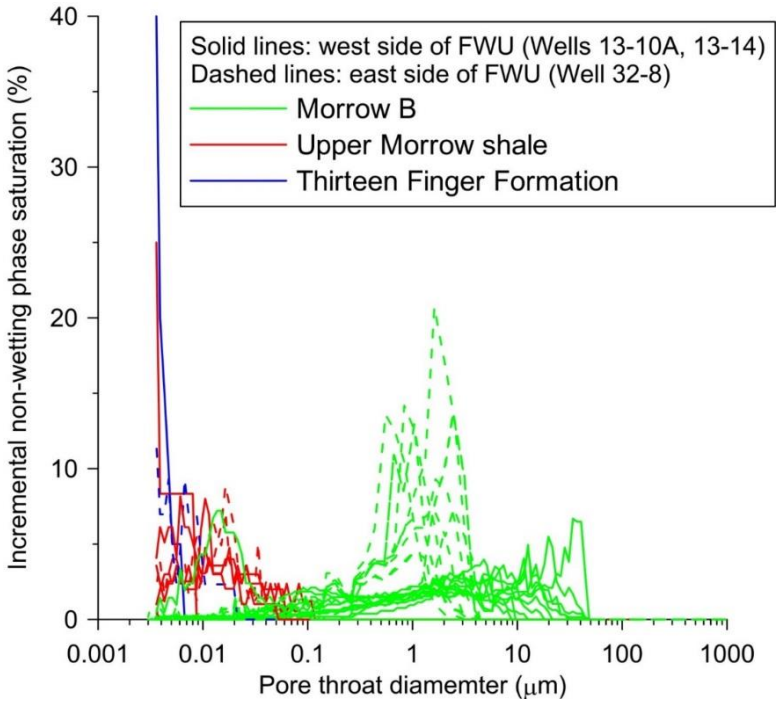

Preprints (www.preprints.org) | NOT PEER-REVIEWED | Posted: 3 February 2021 doi:10.20944/preprints202102.0121.v1

Figure 7. Pore throat diameter in microns vs. incremental non-wetting phase saturation, by formation and well location, determined from mercury porosimetry. Green lines show all data for Morrow B sandstone, red lines show all data for upper Morrow shale, and blue lines show data for Thirteen Finger Limestone.

As discussed by [2], this bimodal distribution reflects abundant diagenetic microporosity in the Morrow B sandstone that exerts a first order dependence on multiphase flow properties of the sandstone flow units. The upper Morrow shale has much smaller pore throat diameters than the Morrow B sandstone ranging from 0.003 to 0.1 μm (Figure 7). The breakthrough pressure for the upper Morrow shale is much higher, ranging from 52.3 to 68.6 MPa (7589 to 9956 psi). The average pore throat diameter for the upper Morrow shale is 0.023 μm with a median of 0.026 μm. The pore apertures ranging from 0.003 to 0.1 μm have several peaks for the mudstones from all three wells, and there are notable differences between the east side of the FWU (well 32-8) and the west side of the FWU (wells 13-10A and 13-14) that may reflect diagenetic and/or depositional differences.

The Thirteen Finger Limestone, however, has breakthrough pressures ranging from 140.6 to 413.4 MPa (20399-59965 psi) with a range of pore throat diameters from 0.0047 to 0.0105 μm. The apparatus could not measure the breakthrough pressures for two of the cementstone samples because the pore throat diameters were too small and needed more pressure than the apparatus could sustain. The average pore throat diameter for the Thirteen Finger Limestone is 0.0076 μm with a median of 0.0076 μm. The cementstone lithology within the Thirteen Finger Limestone has the highest breakthrough pressures for the entire caprock at 413.4 MPa (59,965 psi) and has the smallest pore throat diameters. We do note however that difficulty in obtaining core plug samples for the mudstone lithofacies is somewhat biasing in MICP results for the caprock units.

The mercury porosimetry results were used to calculate CO_2 column heights for the caprock and reservoir formations using standard methods [7] and are shown by depth for the three characterization wells in Figure 8. The CO_2 column heights for the upper Morrow Shale and the Thirteen Finger Limestone range from 1000 m to 10000 m (3280-32808 ft). The cementstone lithology in the Thirteen Finger Limestone has 11000 m of CO_2 column height, with an average of 9000 m (29527 ft). Two of the cementstone samples reached the upper limit of pressure, 60000 psi (414 MPa), that the MICP instrument is capable of sustaining with no intrusion of mercury.

The mudstone lithologies within the upper Morrow shale and Thirteen Finger Limestone have an average CO_2 column height of 2900 m (9514 ft), with a range of 1000 to 10000 m (3280-32808 ft). Not unexpectedly, the caprock CO_2 column height values are 1-to-2 orders of magnitude larger than the sandstone reservoir values and exceed the reservoir thickness, suggesting an excellent caprock integrity. The CO_2 column heights for the Morrow B sandstone reservoir ranged from about 1 to 100 m (3.3-328 ft). These results would suggest that the Morrow shale and Thirteen Finger Limestone caprock should provide excellent capillary sealing for CO_2 for CCUS operations in the FWU. Note that these results refer to the lithologic properties of the rock matrices themselves; to examine further the question of caprock integrity we need to examine in detail the potential of various seal by pass systems both in the form of existing natural fractures and in the potential for inducing fractures during injection and operation phases of CCUS-EOR.

Preprints (www.preprints.org) | NOT PEER-REVIEWED | Posted: 3 February 2021 doi:10.20944/preprints202102.0121.v1

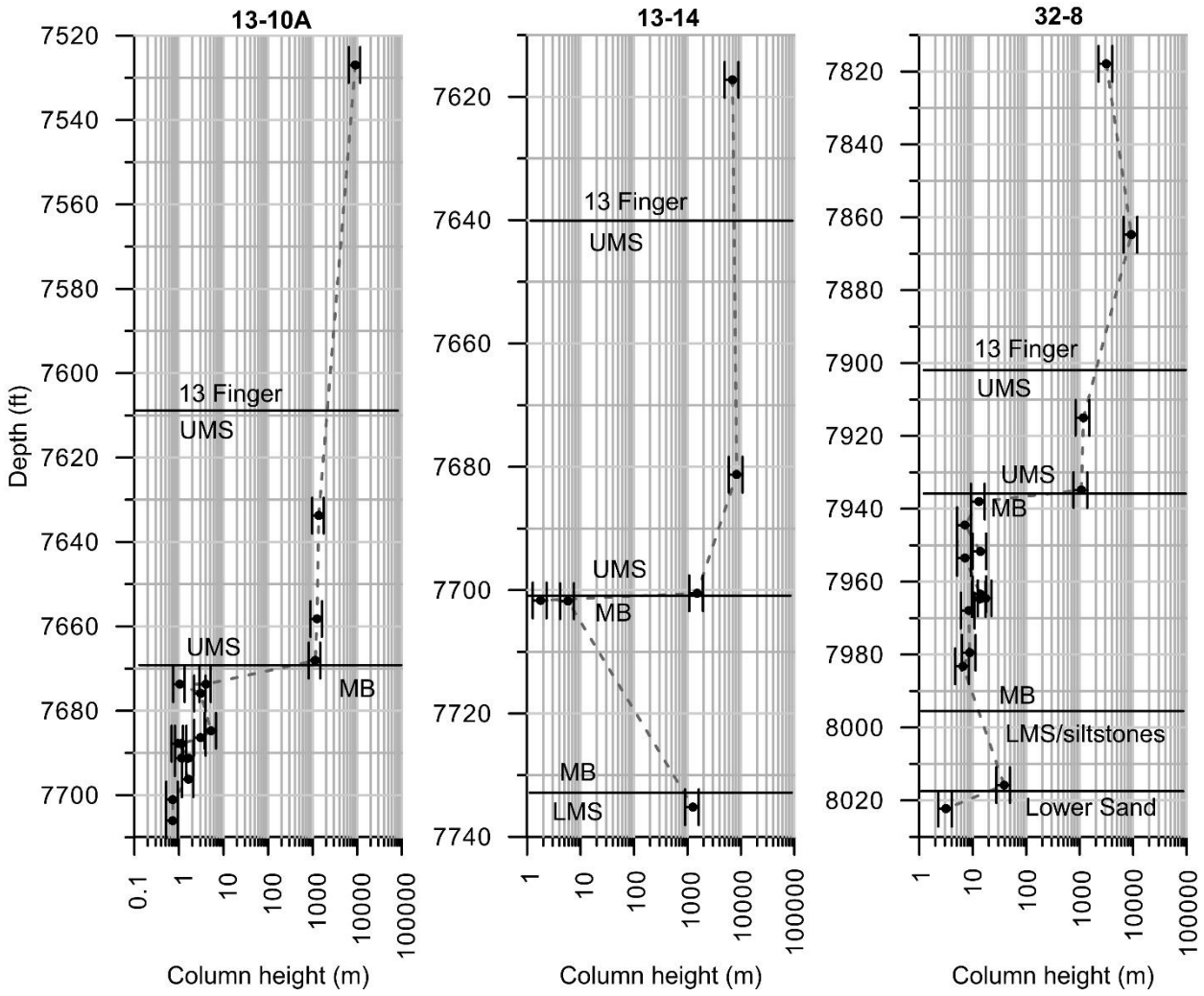

Figure 8. CO_2 column heights for Wells 13-10A, 13-14, and 32-8 determined from MICP analysis.

4.2 Seal Bypass Potential for Farnsworth Caprock Lithologies

4.2.1 Natural and Induced Fractures

Natural fractures in mudstone lithologies can impact fluid-flow, fracture permeability, and mechanical strength of the rock [35], all critical aspects for caprock integrity. For the purposes of understanding how natural fractures impact the ability of FWU caprock lithologies to prevent CO_2 leakage, we need to characterize fracture apertures and density as well as orientation spatially and in reference to current in situ stress orientations. Orientation aspects are especially relevant as: 1. fractures are generally strength-limiting at above-core length scales, and the increase in pore pressure can induce slip and permeability increases for suitably oriented fractures [36,37], 2. fracture orientation with respect to the in situ local stress tensor affects aperture width and thus permeability, and 3. fractures induced by fluid injection, i.e., hydrofractures, propagate in directions dictated by the local stress tensor. It is also important to distinguish fractures induced by coring, as these are not indicative of the state of fracturing in the subsurface, but additionally can aid in determining orientations of principal stresses in the subsurface as described below.

Preprints (www.preprints.org) | NOT PEER-REVIEWED | Posted: 3 February 2021 doi:10.20944/preprints202102.0121.v1

Fractures in FWU caprock were described via fracture class type, orientation, fracture dip, type of mineral fill, fracture porosity, fracture spacing and intensity for wells 13-14 and 32-8 [38,39]. For well 13-14 core, detailed analysis of macroscopic fractures was conducted on nearly 270 feet of continuous whole core material, approximately 123 feet of which contain significant fractures. For our purposes here, we on focus fracture data from well 13-14 in the interval corresponding to the upper Morrow shale as it is the primary caprock lithology, and well 13-14, being in the western portion of the FWU, is where CO_2 injection is monitored by the SWP.

There are four types of fracture classes identified in 13-14 that include: drilling or coring induced fractures; open, low angle shear fractures; high-angle partially open fractures that heal through a carbonate interval; and filled fractures, generally low angle. Drilling-induced fractures are the most abundant. Mineralized fractures are rare, but where recognized the most common mineral in-fill is calcite. Rose diagrams indicating relative fracture orientation of all observed fractures in the Morrow Shale were created for each fracture class and shown in Figure 9. The natural fractures in 13-14 show

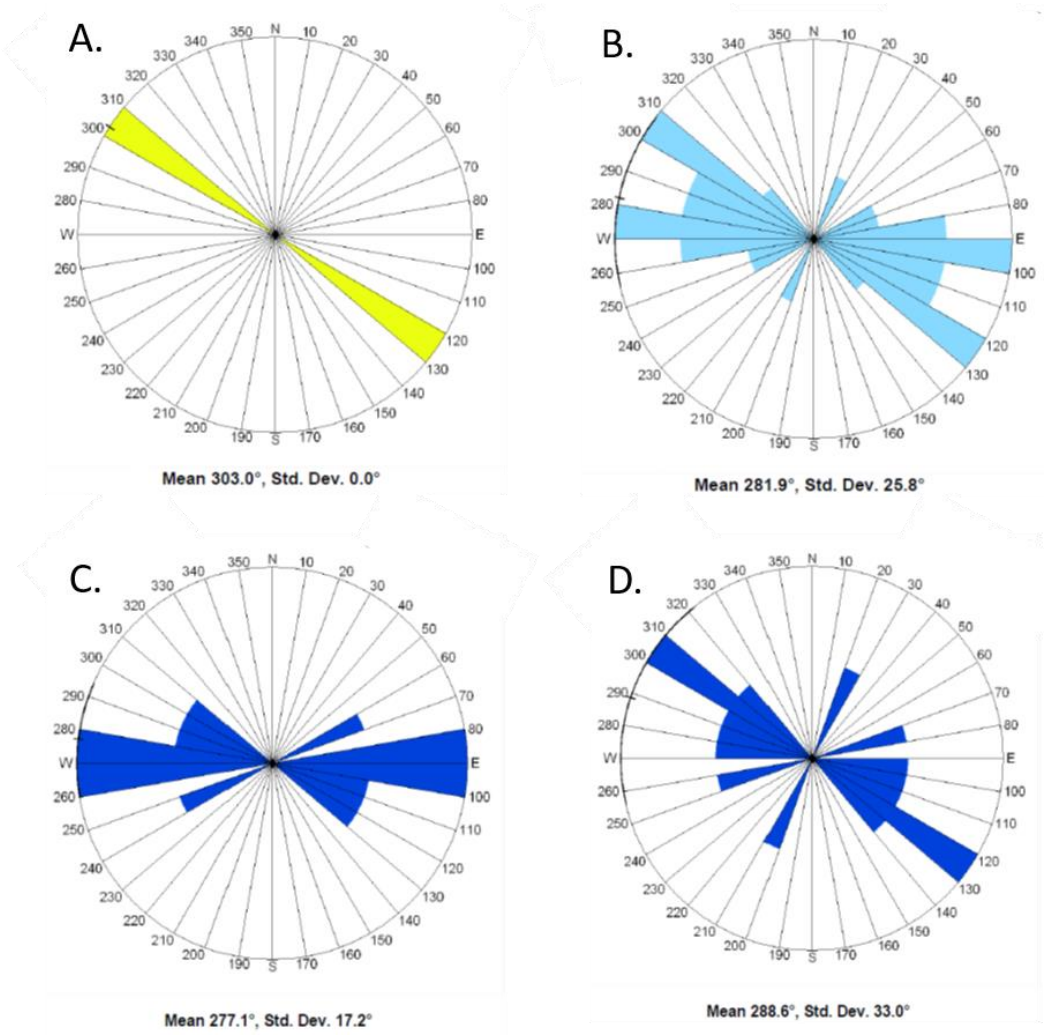

Figure 9. Strike rose diagrams fracture observations in Well 13-14 for the Morrow Shale (7660-7722 feet). A. Coring-induced fractures; B. All natural fractures; C. Open fractures; and D. Partially or totally mineralized fractures. The coincidence in directions between coring induced fractures and natraul fractures existing at FWU suggests the stress conditions resulting in the natural fractures

Preprints (www.preprints.org) | NOT PEER-REVIEWED | Posted: 3 February 2021 doi:10.20944/preprints202102.0121.v1

were of similar orientation, and that natural fractures occuring in the FWU caprocks would be kept open under current subsurface stress conditions.

a similar orientation to the induced fractures and may indicate that the timing of the natural fractures to be more recent, i.e. formed under current stress orientations. According to Snee and Zoback's [40] stress map of Texas (see also [10]), the FWU should be located in a transitional stress state between a normal faulting regime and a strike-slip faulting regime where the maximum horizontal stress (S_H) is slightly less but approaching the vertical stress Sv in magnitude (i.e., S_H max~S_v > S_h where Sh is the minimum horizontal stress). The orientations of maximum horizontal stress in the Texas Panhandle, determined from horizontal breakouts, trend from SE-NW to EW, which would be the expected orientations of hydrofracture propagation as well as open fractures (which open in a direction parallel to the least horizontal compressive stress). These are similar orientations to those of observed open and induced fractures in the Morrow Shale from well 13-14 in Figure 9.

If these are indeed characteristic of natural fracture orientations at FWU, and if we understand the orientations of the principal stress directions, we can then determine critical dip directions for existing fractures that might be induced to slip upon pore pressure increases associated with injection. This is beyond the scope of the present chapter but will be addressed in a later work. However, the coincidence of the coring induced fractures and the natural fractures would suggest that these fractures would be of a critical orientation for slip (i.e. shear fracture) associated with fluid-injection induced overpressure. What bodes well for caprock integrity, however, is the relative rare occurrence of fractures overall in the FWU caprock lithologies.

4.2.2 Static and Dynamic Mechanical Behavior

It is important to understand the limiting strength of the shallow crust posed by existing fractures [37], and as well is it necessary to understand the heterogeneity in matrix rock mechanical properties. Static rock mechanics properties concern poroelastic deformation, yielding, and ultimate rock strength and failure. A typical suite of rock mechanics tests that permit parameterization of constitutive models includes an unconfined compression (UCS) test (a right cylinder of rock is exposed to an axial load with no confining load applied to the round surface of the cylinder), several triaxial (TXC) tests (an axial load is applied to the long axis of the cylinder with a constant confining pressure applied to the cylinder sides), and a hydrostatic test in which the rock cylinder is subject to a constant applied pressure, with or without separately controlled pore pressure. A deformable jacket surrounding the cylinder keeps the pore and confining systems separate. These tests allow us to examine the variability of elastic properties (i.e., Young's Modulus and Poisson's Ratio, which can either be used to represent an elastically isotropic medium, or be directionally dependent, which is a simplified means to assess elastic anisotropy, for example with respect to primary bedding direction), yielding behavior (involving inelastic processes such as microfracture growth and coalescence, or pore collapse), and failure (involving complete loss of cohesion of a deforming rock generally by a through-going shear fracture).

An extensive suite of geomechanical properties have been assembled from the Terra Tek testing program for the FWU characterization wells and are available in the series of Terra Tek reports [41-43]. One valuable aspect of the data set is the degree to which it maps properties on rock units based on Terra Tek's HRA methodology for sampling and testing. We focus here on elastic properties,

Preprints (www.preprints.org) | NOT PEER-REVIEWED | Posted: 3 February 2021 doi:10.20944/preprints202102.0121.v1

failure envelopes and fracture gradients as they concern caprock integrity, but this array of geomechanical data can be used for, among other things:

- Advanced elastic-plastic modeling of yielding and failure associated with CO_2 injection and plume migration;
- Biot and compressibility parameters for reservoir engineering;
- Determination of "frac" gradients to guide injectivity and pressure management strategies for risk and performance assessment.
- Guiding modeling for estimating surface expressions of CO_2 injection such as uplift and subsidence for monitoring and verification efforts.
- Inform monitoring of induced microseismic activity during injection.
- Aid in construction of velocity models for seismic inversion.
- Aid in determining caprock integrity for risk and performance assessments.

Static and dynamic elastic properties are represented as continuous profiles that combine well logging, Terra Tek's HRA analysis, and laboratory measurements on core that are used for calibration. These are presented in Figures SM-3, -4, and -5 in the Supplemental Materials. In this section we detail static rock mechanics properties by well and implications for caprock integrity. Static horizontal and vertical Young's Modulus and Poisson's ratio as interpreted from combining

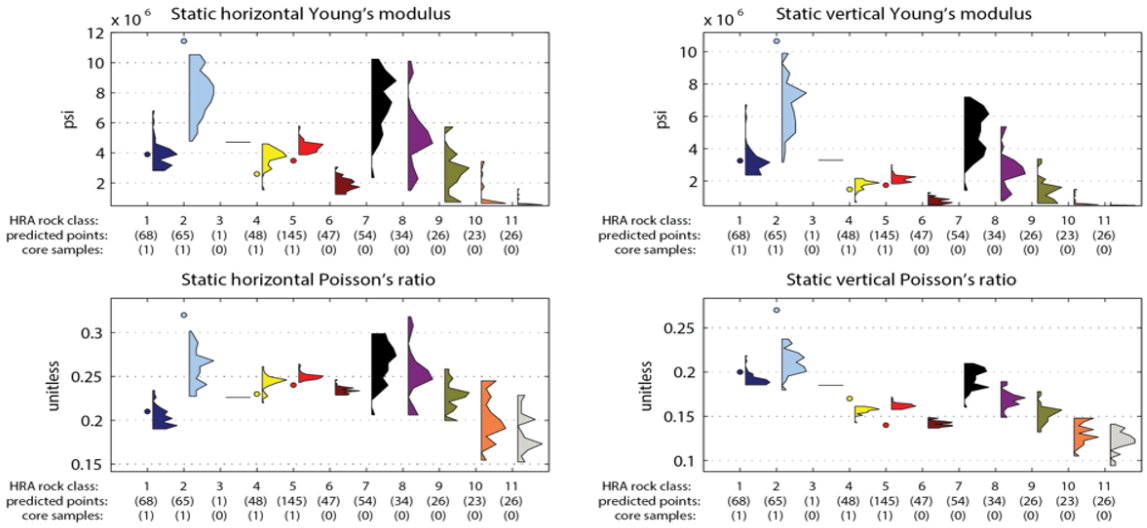

Figure 10. Static Young's Modulus (**Top**) and Poisson's Ratio (**Bottom**) determined by combining ranges interpreted from well log static rock compression tests illustrating the contrast in elastic properties of the Morrow B sandstone reservoir and the Morrow shale and Thirteen Finger Limestone caprock for well 13-10A. The left-hand figure shows values for samples oriented horizontally, and the right figure shows values for samples oriented vertically. In general, horizontal values are slightly higher than vertical values, reflecting an anisotropy likely derived from depositional fabrics.

values from sonic well logs with values determined from laboratory static testing for Well 13-10A are shown by rock class in Figure 10. In general, horizontal values are slightly higher than vertical values, reflecting an anisotropy likely derived from depositional fabrics. The highest values (with light blue) are found in the Thirteen Finger Limestone lithofacies, the next highest correspond to the black color (Bcm facies in the Thirteen Fingers Limestone) whereas the lowest values (orange and grey) are weaker Bcm lithofacies in the Thirteen Fingers Limestone. Morrow B sandstone lithofacies (dark

Preprints (www.preprints.org) | NOT PEER-REVIEWED | Posted: 3 February 2021 doi:10.20944/preprints202102.0121.v1

Blue) and Morrow shale (yellow, red, and brown) lithofacies are intermediate in value. In general, this is not an unexpected degree of elastic heterogeneity, but could influence how the caprock responds to a reservoir-scale increase in pore pressure associated with CCUS activities.

Probably more important for caprock integrity is the failure behavior of the suite of rock types. Figures 11 shows Coulomb failure envelopes for Thirteen Finger Limestone and Morrow shale caprock and Morrow B sandstones created by combining UCS and triaxial test data for these rock types. Figure 11A and B show the shear dilatant behavior of the weaker rock types tested, Blm mudstones from the Thirteen Finger Limestone (rock class Orange as shown in Figure 4) in Figure 11A, and from the Morrow shale (rock class Red, a laminated mudstone as shown in Figure 4). The two mudstones behave very similarly, with an angle of internal friction ϕ equal to 27°, and an apparent cohesion of around 3500 psi. A slightly weaker shale tested was a silty mudstone from the Morrow shale (Figure 11C, rock class Yellow) with a lower ϕ of 21° and an apparent cohesion of ~3200 psi.

Morrow B sandstones are apparently much weaker, as shown in Figure 11D. The sandstones have a greater ϕ of 44°, but a very low cohesive strength of 830 psi. This analysis shows that

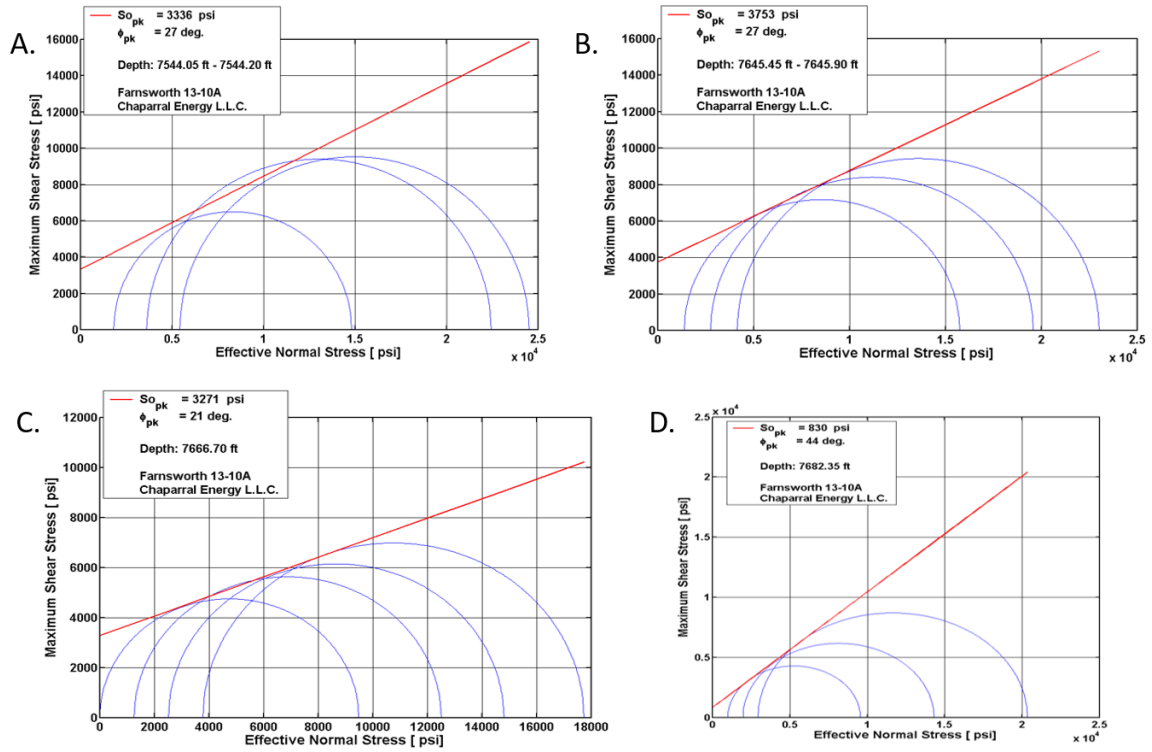

Figure 11. Example Coulomb failure envelopes for Well 13-10A. **(A.)** Coulomb failure envelope (i.e., shear dilatant failure) measured during triaxial compression testing of samples from HRA Unit Orange (7544.05 - 7544.20 ft, Thirteen Fingers). Linear failure parameters of cohesion and friction angle are provided for failure (peak values). **(B)** Same as A except for HRA Unit Red (7645.45 - 7645.90 ft , Morrow Shale). **(C)** Same as B and C except for HRA Unit Yellow (7666.70 ft, Morrow shale). **(D)** Same as A, B, and C except for HRA Unit Dark Blue (7682.35 ft, Morrow B sandstone).

the sandstones of the Morrow B subjected to in situ stress conditions below the failure envelopes in Figure 11 would be more highly likely to experience shear failure associated with fluid injection than the mudstone formations. This is suggested as well by Brazil tensile failure tests for the Morrow B

 doi:10.20944/preprints202102.0121.v1

sandstone, Morrow shale, and Thirteen Finger Limestone discussed by Trujillo ([10], her Figure 35), which show that the caprock lithologies in general have two to four times the tensile strength as compared to the Morrow B sandstones. Trujillo [10] also shows that a sample of cementstone from the Thirteen Finger Limestone has apparently an incredibly high unconfined compressive strength of ~47 kpsi, which is approaching that of some crystalline rocks.

4.2.3 Fracture Gradients in Farnsworth Reservoir and Sealing Lithologies

We bracketed the orientation of the three principal stresses within the FWU from both regional observations [40] and observations of open and induced fractures in the Morrow shale. There is a vertical maximum principal stress, a minimum horizontal stress in the orientation of 350° (North-South), and a maximum horizontal stress orientation at about 270° (East-West). A more difficult determination is an assessment of magnitude of the principal stresses (vertical/overburden stress (Sv), the maximum horizontal stress (SH), and the minimum horizontal stress (Sh)), and addressing this is beyond the scope of this chapter. However, based on the rock mechanics testing data, we can bracket the minimum horizontal stress gradient required to exceed rock strength and propagate fractures. These estimates are typically used to limit the extent of injection-associated pore fluid overpressures so as to not damage formations during injection and production activities. For CCUS in the FWU, these values are important to consider; based on the in-situ stress orientations in the FWU, any fractures created in the weaker reservoir lithology would be oriented vertically, because the minimum principal stress is horizontal.

Preprints (www.preprints.org) | NOT PEER-REVIEWED | Posted: 3 February 2021 doi:10.20944/preprints202102.0121.v1

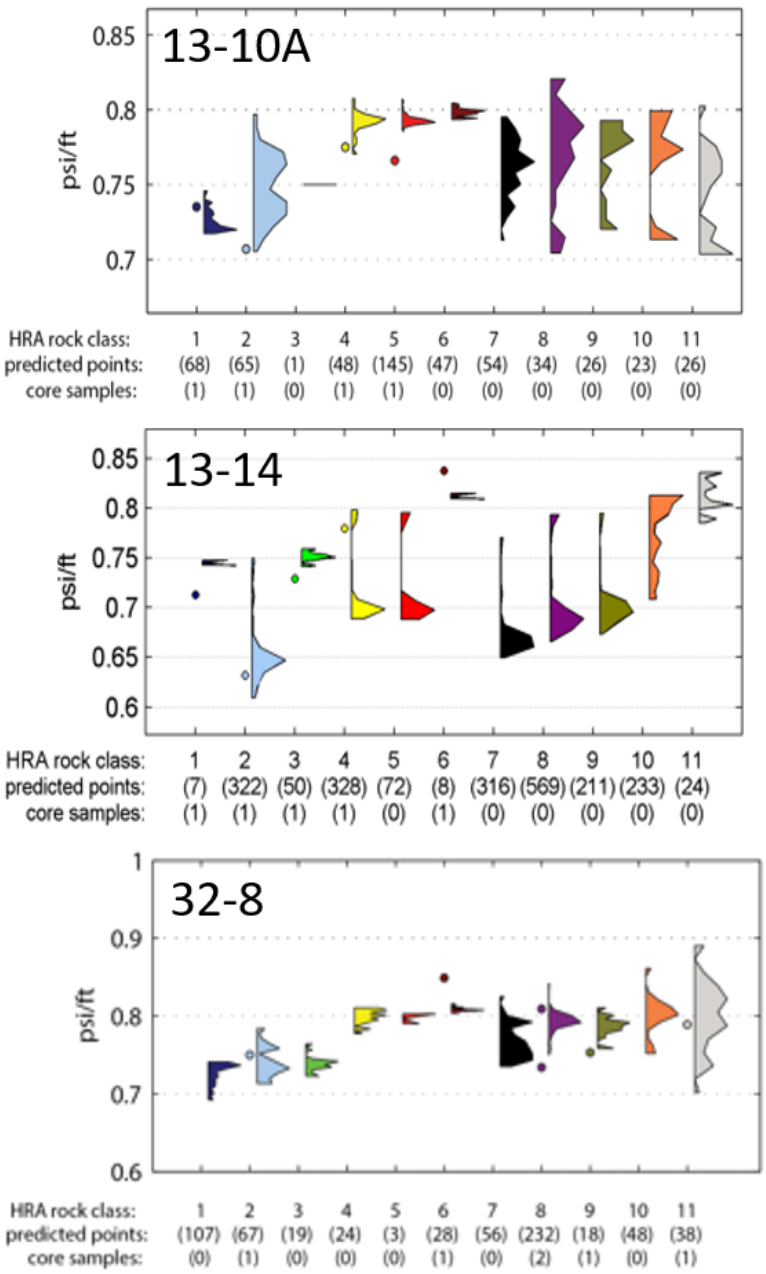

Figure 12. Estimated minimum horizontal stress (fracture) gradients by rock class for each of the three characterization wells. In general the Morrow B sandstone rock classes (light and dark blue) have lower values indicating they are more easily fractured. Propogating vertical fractures associated with injection-induced hydrofracturing would likely not propogate into the overlying caprock formations.

Estimates of the minimum horizontal stress gradient in FWU caprock and reservoir lithologies is determined from the Terra Tek suite of testing summarized in the Figure SM-3, 4 and 5 and are shown in Figure 12 for all three characterization wells. The lowest values are in the well 13-14, but in general values cluster around 0.70 to 0.80 psi/foot (1 psi/ft is equivalent to 0.0226 MPa/m). While some of the lowest values are in the caprock lithologies, so are the highest values, with the Morrow B sandstones falling generally below 0.75. Pore pressure gradients range from 0.43 psi/ft in the Thirteen Finger Limestone and increase to 0.585 psi/ft in the upper Morrow Shale [10], while an estimated vertical stress gradient is 1.1 psi/ft. With a fracture gradient of 0.7 psi/ft at a depth of 7700 ft in the

Preprints (www.preprints.org) | NOT PEER-REVIEWED | Posted: 3 February 2021 doi:10.20944/preprints202102.0121.v1

reservoir, the maximum pore pressure that could be attained within the reservoir without fracture is ~5390 psi or ~ 37 MPa. At the caprock-reservoir interface the fracture gradient is 0.85 psi/ft at a depth of 7668 feet, the maximum pore pressure that could be attained within the caprock without fracture is~6518 psi (~ 44.9 MPa). Reservoir pressures are currently at 4500-4700 psi (31–32 MPa) in the eastern portion of the FWU (likely a result of water flooding), and injection-induced pressures by the CO_2 in the western portion of the field are on the order of 5000 psi (34.5 MPa), which is well below the maximum level. The fracture gradients indicate that the Morrow B sandstone reservoir is weaker than the overlying lithologies, so any fracture initiated around CCUS injection wells in the FWU should not propagate into the overlying sealing units.

4.3 Seal Lateral Continuity in the Farnsworth Unit

Isopach maps of the upper Morrow shale and Thirteen Finger Limestone across the FWU were prepared from formation tops and bottoms after data compiled by [9] and are shown in Figure SM-6 in the Supplemental Material, along with the total caprock thickness. The minimum thickness for the upper Morrow shale occurs in the middle of the FWU at ~42 ft. The minimum thickness of the Thirteen Finger Limestone occurs in the western portion of the FWU at around 60 ft. In general, the caprock thickness ranges from 240 ft in the eastern portion to ~120 feet in the western portion of the FWU. The lateral caprock continuity easily suggests that seal integrity would be anticipated along the mapped extent of the FWU.

4.4 Caprock Integrity Inferred from Noble Gas Analyses

Measurement of naturally occurring noble gases in a vertical profile from preserved fresh core in the reservoir and caprock units complements the other caprock integrity analyses as the pattern of noble gas isotopic contents is the direct in situ integrated result of the driving forces and transport properties through the reservoir and the caprock. Thus, the noble gas isotopic profile reflects original infiltration of groundwater with atmospheric noble gas contents and the addition of subsurface geogenic noble gases, which are affected by transport via advection and/or diffusion and potentially more recent reservoir activities since the water flooding began in the 1950's. Noble gas profiles that reflect diffusion-dominated transport are expected for high sealing quality caprock, whereas caprock with seal bypass systems (i.e., an interconnected fracture network) may result in an advective noble gas profile.

Context for interpreting noble gas data measured in this study is that atmospherically sourced isotopes are ^{20}Ne and ^{36}Ar, whereas geogenic isotopes sourced in the subsurface are ^{3}He, ^{4}He, ^{40}Ar, and ^{22}Ne [44]. Isotopic ratios for atmospheric, crustal, and mantle reservoirs are well known and used to identify sources of fluids in petroleum systems [45]. The measured ^{3}He over ^{4}He ratio (R) from FWU samples, normalized by that same ratio for the atmosphere (R_a), have values of ~ 0.02 for most measurements within the Thirteen Finger Formation and the upper Morrow shale (Figure 13, see the left-most column; values are listed in Table SM-7 in the Supplemental Materials). These values of ~0.02 are consistent with crustal fluids—the crustal end-member R/R_a value is 0.02, which represents the dominant production of ^{4}He from U and Th decay [45]. Deviations from values of ~0.02 occur within the Morrow B sandstone and near the top of the Thirteen Finger Formation (Figure 13).

The Morrow B sandstone deviations from 0.02 R/R_a are most likely caused by the long-term water flooding in the Farnsworth Unit, which initially used groundwater sourced from the Ogallala

Preprints (www.preprints.org) | NOT PEER-REVIEWED | Posted: 3 February 2021 doi:10.20944/preprints202102.0121.v1

Formation that probably had R/R_a values at closer to 1.00 than the older caprock fluids (younger groundwaters will probably have values closer to one than older crustal fluids; see [45]. The R/R_a value greater than 1.00 in the Morrow B sandstone may be an artifact of the laboratory analysis; mantle-sourced fluids have R/Ra values much greater than one [45], but this is unlikely as a source due to the rest of the samples being less than one. Complex phase partitioning between groundwater, oil, and any gas phase may also lead to ratios greater than one. Ratios of $^4He/^{20}Ne$, normalized by the atmospheric value, are several orders of magnitude greater than one for most samples, thus indicating high helium concentrations due to long-term production of ^4He from U and Th in the sealing lithologies with low permeability and low effective diffusivity. The very distinct change in R/R_a from the Morrow B into the upper Morrow shale indicates that the upper Morrow shale is a good seal at least at that contact measured by the coring.

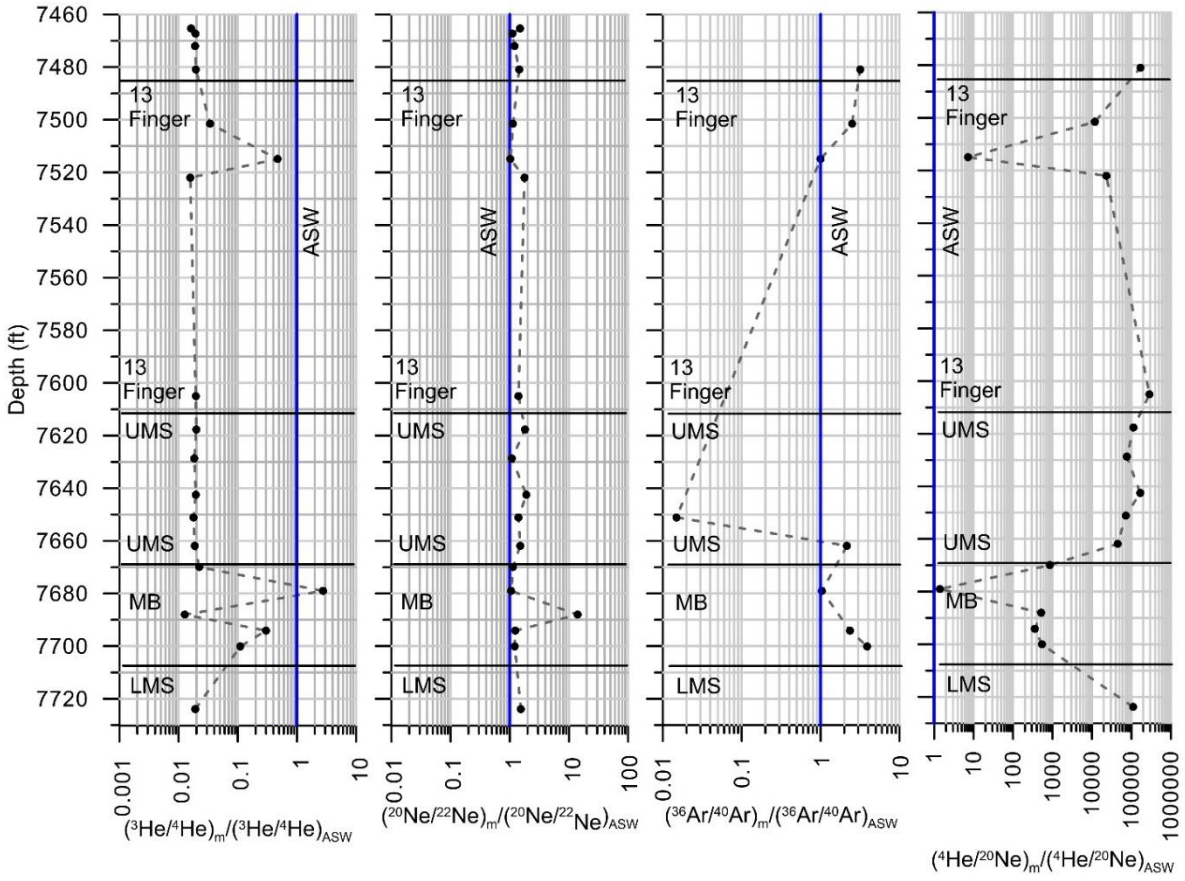

Figure 13. Noble gas ratios versus depth for Well 13-10A. The subscript *m* stands for the ratio measured for the sample, whereas the subscript *ASW* stands for the air saturated water value for the ratio.

Because of the high amount of methane and helium in many samples as observed during laboratory analysis, sample splitting was necessary, which affected the reliability of the argon values. Thus, argon values were not reported by the laboratory for several samples (Table SM-7). The argon isotopic values that are available also reflect some process that introduce fluids into the system that may have been in equilibrium with the atmosphere (Figure 13). A sample within the upper Morrow

Preprints (www.preprints.org) | NOT PEER-REVIEWED | Posted: 3 February 2021 doi:10.20944/preprints202102.0121.v1

shale has a relatively low light-to-heavy Ar isotopic ratio, which is expected as ^{40}K within the formation would produce ^{40}Ar.

The deviations from 0.02 R/R_a for the Thirteen Finger Formation may be due to improper sealing or leakage of the preservation canisters as such leakage would bring the values closer to 1.00, which may be likely for the sample at depth 7,515 ft (2290.57 m) as its R/R_a is 0.47, and its neon and argon isotope ratios are close to the atmospheric values (Figure 13). However, the adjacent sample at depth 7,502 (2286.01 m) also has a relatively high R/R_a of 0.034 and its neon and argon ratios are slightly shifted from the atmospheric equilibrium values. Thus, it is possible that some process is occurring near the top of the Thirteen Finger Formation to introduce a minor atmospheric source of fluids or is otherwise fractionating the noble gases. We speculate that the observed natural fractures may permit fluid movement that has larger R/R_a than the crustal values of ~0.02 of the rest of the Thirteen Finger Limestone and upper Morrow Shale samples. This would suggest that while the upper Morrow shale and lower Thirteen Fingers Limestone appear to have been isolated from surrounding fluid movement (and fluid contamination associated with decades-long water flooding operations at FWU), the upper portions of the Thirteen Fingers Limestone may have been infiltrated by fluids in contact with atmospheric noble gas isotopic values.

5. Discussion

Direct formation-scale assessment of caprock integrity is difficult. Core-based measurements, wire-line logging, and seismic techniques are: very localized and/or may lack resolution to identify potential seal-by systems (e.g., such as connected fracture networks that are below seismic resolution); or used to infer large-scale behavior, which may include modeling to integrate to the reservoir and caprock properties made at different locations and different scales [46]. To build confidence in and understanding of caprock integrity at FWU, this study by the Site Characterization team of the SWP approaches caprock integrity by systematically assessing processes that govern sealing quality at different scales following the framework of Figure 1. Thus, the processes are examined from nanoscale capillary-wettability controls to mechanical properties and the full caprock-reservoir system behavior via sedimentological-stratigraphic evaluation and large-scale in situ noble gas transport. Small-scale sealing integrity is confirmed by MICP measurements of high breakthrough pressures and very high estimated CO_2 column heights for the upper Morrow shale and the Thirteen Finger Limestone. Mechanical properties from core measurements indicate that, while the Morrow B sandstone is relatively weak, fractures that may be induced from CO_2 injection activities would probably not propagate into the upper Morrow shale. The naturally occurring in situ noble gas isotopic profile builds confidence that water flooding and production reservoir operations prior to coring of Well 13-10A did not damage a high-quality sealing caprock as the helium ratios are quite different across the Morrow B sandstone and upper Morrow shale contact. The thickness and lateral continuity of the upper Morrow shale and Thirteen Finger Limestone further strengthen the likelihood of a high-quality sealing caprock system.

6. Conclusions

Our main conclusions from this study are as follows:

 doi:10.20944/preprints202102.0121.v1

- An extensive suite of petrophysical and geomechanical data, linked to lithologic heterogeneity at Farnsworth, can inform reservoir and geomechanical modeling of CO_2 injection, storage, and EOR efforts at Farnsworth:
- MICP results show that sealing units in the Morrow Shale and Thirteen Finger Limestone units should provide excellent sealing capacity for storage of CO_2 in the Morrow B Sandstone injection unit, as calculated CO_2 column heights exceed the thickness of the Morrow B.
- Cementstones in the Thirteen Fingers have anomalously high sealing potential and strength, and the ability of these thin bands of tight carbonate to serve as seals by themselves would be limited only by their lateral continuity.
- Failure analyses show that the Morrow B sands are weaker than overlying lithologies, so that any fracture initiation around the injection well would not be expected to propagate into the overlying sealing units.
- A preliminary assessment of fracture gradient shows that formations should larger be able to support injection and overpressure to ~5000 psi, a few thousand psi over hydrostatic pressure values at the depths of interest.
- Noble gas analysis from fresh core shows that the caprock lithologies show no degree of leakage from historical water and CO_2 flooding in the FWU, whereas the Morrow B sandstone shows an impact from EOR activities.

Together, these analyses conducted at different scales strongly suggest an excellent sealing capacity for the Morrow Shale and Thirteen Fingers lithologies. This is from both the high degree of capillary sealing, the low potential for seal bypass, and the large regional extent of the caprock lithologies in the FWU.

Supplementary Materials: The following are available online at www.mdpi.com/xxx/s1: Tables: Table SM1-SM-3: Caprock thin section petrologic descriptors with Schlumberger Heterogeneous Rock Classification (HRA) assigned unit color; Table SM-4. Summary of petrophysical properties (Terra Tek routine core analysis); Table SM-5. Terra Tek Tight rock analysis for mudstone and limestone lithofacies in the Morrow Shale and Thirteen Fingers Limestone. Table SM-6. Mercury intrusion data and associated analysis by rock class for the 13-10A, 13-14, and 32-8 characterization wells. Table SM-7. Results of noble gas analysis, including the sample mass and supplementary estimates of wet bulk density, total porosity based on laboratory analysis on fresh core samples or well log interpretation. Figures: Figure SM1. Well 13-14 HRA summary and accompanying well logs used in analysis; prepared by Schlumberger; Figure SM-2. Well 32-8 HRA summary and accompanying well logs used in analysis; prepared by Schlumberger; Figure SM-3. Well 13-10A interpolated static and dynamic rock mechanics properties based on Schlumberger/Terra Tek HRA log analysis and lab experiments (shown as red and black dots); Figure SM-4. Well 13-14 interpolated static and dynamic rock mechanics properties based on Schlumberger/Terra Tek HRA log analysis and lab experiments (shown as red and black dots); Figure SM-5. Well 32-8 interpolated static and dynamic rock mechanics properties based on Schlumberger/Terra Tek HRA log analysis and lab experiments (shown as red and black dots); Figure SM-6. Isopach maps of caprock lithologies in the Farnsworth Unit. A. Morrow shale B. Thirteen Finger Limestone. C. Total caprock thickness (after Rose-Coss, 2017).

Author Contributions: Conceptualization, M.C., J.E.H., P.S.M.; methodology, J.E.H., P.M., T.A.D.; formal analysis, N.T., D.R.-C.., J.E.H.; investigation N.T., D.R.-C..; data curation, J.E.H.; writing—original draft preparation, N.T., D.R.-C., P.M..; writing—review and editing, T.A.D., J.E.H., M.C..; supervision, M.C., P.M., J.E.H..; project administration, M.C., W.A..; funding acquisition, M.C., W.A.. All authors have read and agreed to the published version of the manuscript.

Funding: Funding for this project was provided by the U.S. Department of Energy's (DOE) National Energy Technology Laboratory (NETL) through the Southwest Regional Partnership on Carbon Sequestration under Award No. DE-FC26-05NT42591.

Acknowledgments: We thank Steve Cather for his lithologic interpretations found in Tables SM-1 through 3 in the Supplemental Material. We thank Joseph Hall, a geologist formerly of Chaparral Energy LLC, for assistance in designing the coring program, his geologic expertise of the Farnsworth Unit, and his assistance with characterizing the core. Wayne Rowe of Schlumberger managed well logging efforts for this project. Christopher Gillespie of Terra Tek, formerly a Schlumberger company, managed the myriad geomechanical, geochemical, and petrophysical measurements provided at Terra Tek for this project. Sandia National Laboratories is a multimission laboratory managed and operated by National Technology & Engineering Solutions of Sandia, LLC, a wholly owned subsidiary of Honeywell International Inc., for the U.S. Department of Energy's National Nuclear Security Administration under contract DE-NA0003525. This paper describes objective technical results and analysis. Any subjective views or opinions that might be expressed in the paper do not necessarily represent the views of the U.S. Department of Energy or the United States Government. The core from which samples were collected for this project are housed at the Subsurface Data and Core Libraries of the New Mexico Bureau, Socorro, New Mexico, USA.

Conflicts of Interest: The authors declare no conflict of interest.

References

1. Cartwright J.; Huuse M.; Aplin A. Seal bypass systems. *AAPG Bulletin*, **2007**, *91*, 1141–1166.
2. Rasmussen, L.; Fan, T.; Rinehart, A.; Luhmann, A.; Ampomah, W.; Dewers, T.; Heath, J.; Cather, M.; Grigg, R. Carbon storage and enhanced oil recovery in Pennsylvanian Morrow Formation clastic reservoirs: Controls on oil-brine and oil-CO2 relative permeability from diagenetic heterogeneity and evolving wettability. *Energies*, **2019**, 12, 3663; doi:10.3390/en12193663.
3. Rose-Coss, D.; Ampomah, W.; Hutton, A.C.; Gragg, E.; Mozley, P.; Balch, R.S; Grigg, R. Geologic characterization for CO 2-EOR Simulation: A Case Study of the Farnsworth Unit, Anadarko Basin, Texas. **2015**, American Assoc. Petrol. Geol. Search and Discovery Article #80484, 29p.
4. Ross-Coss, D.; Ampomah, W.; Cather, M.; Balch, R.S.; Mozley, P.; Rasmussen, L. An improved approach for sandstone reservoir characterization. In *SPE Western Regional Meeting*. Society of Petroleum Engineers, May 2016.
5. Ampomah, W.; Balch, R.S.; Grigg, R.B.; Will, R.; Dai, Z; White, M.D.2016, April. Farnsworth Field CO2-EOR project: Performance Case History. *SPE Improved Oil Recovery Conference*. Society of Petroleum Engineers, April 2016
6. U.S. Department of Energy, Office of Basic Energy Sciences, Basic Research Needs for Geosciences: Facilitating 21st Century Energy Systems. Report from the workshop held February 21–23, 2007, https://www.osti.gov/servlets/purl/935430.
7. Heath, J. Multi-Scale Petrography and Fluid Dynamics of Caprocks Associated with Geologic CO_2 Storage. Dissertation, New Mexico Institute of Mining and Technology, 2010, 410 p.
8. Puckette, J.; Al-Shaieb, Z.; Van Evera, E. Sequence Stratigraphy, Lithofacies, and Reservoir Quality, Upper Morrow Sandstones, Northwestern Shelf, Anadarko Basin, In *Morrow and Springer in the Southern Midcontinent, 2005 Symposium*, Andrews, R.D., ed Oklahoma Geological Survey Circular, 2008, 81-97.
9. Rose-Coss, D.A Refined Depositional Sequence Stratigraphic and Structural Model for the Reservoir and Caprock Intervals at the Farnsworth Unit, Ochiltree County, TX. Master's Thesis, New Mexico Institute of Mining and Technology, 2017, 258 p.
10. Trujillo, N. Influence of Lithology and Diagenesis on Mechanical and Sealing Properties of the Thirteen Finger Limestone and Upper Morrow Shale, Farnsworth Unit, Ochiltree County, Texas. Master's Thesis, New Mexico Institute of Mining and Technology, 2017, 83 p.
11. Balch R.; McPherson, B. Phase III Demonstration: Farnsworth Unit, Mastering the Subsurface through Technology Innovation and Collaboration: Carbon Storage and Oil and Natural Gas Technologies Review Meeting, 2016, August 16–18.
12. Hutton, A.C. Geophysical Modeling and Structural Interpretation of a 3D Reflection Seismic Survey in Farnesworth Unit, TX, MS Thesis, NM Institute of Mining and Technology, 2015, 101 pp.
13. Ross, C.A.; Ross, J.P. Late Paleozoic transgressive-regressive deposition. *Society of Economic Paleontologists and Mineralogists, Special Publication*, 1988, *42*, 227-247
14. Higley, D.K.; Cook, T.A.; Pawlewicz M.J. Petroleum Systems and Assessment of Undiscovered Oil and Gas in the Anadarko Basin Province, Colorado, Kansas, Oklahoma, and Texas—Woodford Shale Assessment Units. In *Compiler, Petroleum Systems and Assessment of Undiscovered Oil and Gas in the Anadarko Basin*

Province, Colorado, Kansas, Oklahoma, and Texas—USGS Province 58. Higley DK (ed), 2014, USGS Digital Data Series DDS-69-EE, 24.

15. Perry, W.J., Tectonic evolution of the Anadarko Basin region, Oklahoma: U.S. Geological Survey Bulletin, 1989, 1866-A, p.19.
16. Cather, M.; Rose-Coss, D.; Gallagher, S.; Trujillo, N.; Cather, S.; Hollingworth, S.; Mozley, P.; Leary, R., Deposition, diagenesis, and sequence stratigraphy of the Pennsylvanian Morrowan and Atokan Intervals at Farnsworth Unit, *Energies*, **2021** (this volume).
17. Evans, J.L. Major Structural and Stratigraphic Features of the Anadarko Basin. In *Pennsylvanian Sandstones of the Mid-Continent*. Hyne, N.J. (ed), Tulsa Geological Society, Special Publication, 1979, 1, 97–113.
18. Munson, T. W. Depositional, Diagenetic, and Production History of the Upper Morrowan Buckhaults Sandstone, Farnsworth Field, Ochiltree County Texas, Master's Thesis, West Texas University, Canyon, Texas, 1988, 117 p.
19. Brewer, J.A.; Good, R.; Oliver, J.E.; Brown, L.D.; Kaufman, S.; COCORP profiling across the Southern Oklahoma Aulacogen: Overthrusting of the Wichita Mountains and compression within the Anadarko Basin. *Geology*, **1983**, *11*: 109–114.
20. Ye H.; Royden, L.; Burchfiel, C.; Schuepbach, M. Late Paleozoic deformation of interior North America: the greater ancestral Rocky Mountains: *Am Assoc Pet Geol Bull*, **1996**, *80*, 1397-1432.
21. Marino, S.; Herring, S.; Stevens, K.; Petriello, J.; Handwerger, D.; Suarez-Rivera, R.; Woodruff, W. Integration of quantitative rock classification with core-based geologic studies: Improved regional-scale modeling and efficient exploration of tight shale plays. *Society of Petroleum Engineers* SPE 167048, presented at SPE Unconventional Resources Conference and Exhibition-Asia Pacific, Brisbane, Australia, 11-13, November 2013.
22. Dullien, F.A.L, Porous Media: Fluid Transport and Pore Structure, 2nd ed.; Academic Press, San Diego, California, USA, 1992, 574 p.
23. Dewhurst, D.N.; Jones, R.M.; Raven, M.D., Microstructural and petrophysical characterization of Muderong Shale: Application to top seal risking. *Petroleum Geoscience*, **2002**, *8*, 371-383.
24. Ingram, G.M.; Urai, J.L.; Naylor, M.A. Sealing processes and top seal assessment. *Norwegian Petroleum Society Special Publications*, **1997**, *7*, 165-174.
25. Heath, J.E.; Dewers, T.A.; McPherson, B.J.O.L.; Petrusak, R.; Chidsey, Jr., T.; Rinehart, A; Mozley, P. Pore networks in continental and marine mudstones: Characteristics and controls on sealing behavior. *Geosphere*, **2011**, *7*, 429-454, doi: 10.1130/GES00619.1.
26. Iglauer, S.; Salamah, A.; Sarmadivaleh, M.; Liu, K.; Phan, C. Contamination of silica surfaces: impact on water-CO_2-quartz and glass contact angle measurements. *Int. J.Greenhouse Gas Control*, **2014**, *22*, 325–328.
27. Osenbrück, K.; Lippmann, J.; Sonntag, C. Dating very old pore waters in impermeable rocks by noble gas isotopes. *Geochimica et Cosmochimica Acta*, **1998**, *62*, 3041–3045.
28. Hendry, M.J.; Kotzer, T.G.; Solomon, D.K. Sources of radiogenic helium in a clay till aquitard and its use to evaluate the timing of geologic events. *Geochimica et Cosmochimica Acta*, **2005**, 69: 475–483.
29. Sonnenberg, S.A.; Shannon, L.T.; Rader, K.; von Drehle, W.F.; Martin, G.W., Regional Structure and Stratigraphy of the Morrowan Series, Southeast Colorado and Adsjacent Areas. *In Morrow Sandstones of Southeast Colorado and Adjacent Areas,* 1990, Rocky Mountain Association of Geologists Guidebook, pp. 37-50. 1990
30. Bagley, M.E.; Puckette, J.; Boardman, D.; Watney, W.L. 2001, Lithofacies and reservoir assessment for the Thirteen Finger Limestone, Hugoton Embayment, Kansas. 2001 Poster, AAPG Search and Discovery Article #50513.
31. Petriello, J.; Marino, S.; Suarez-Rivera, R.; Handwerger, D. A.; Herring, S.; Woodruff, W.; Stevens, K. Integration of Quantitative Rock Classification with Core-Based Geologic Studies: Improved Regional-Scale Modeling and Efficient Exploration of Tight Shale Plays, 2013, Paper 167048-MS presented at SPE Unconventional Resources Conference and Exhibition-Asia Pacific, Brisbane, Australia , 11-13 November.
32. Suarez-Rivera, R.; Handwerger, D.; Rodriguez-Herrera, A.; Herring, S.; Stevens, K.; Vaaland Dahl, G.; Borgos, H.; Marino, S.; Paddock, D. Development of a heterogeneous Earth model in unconventional reservoirs for early assessment of reservoir potential, ARMA 13-667, 47th US Rock Mechanics/Geomechanics Symposium held in San Francisco, California, USA, 23-26 June, 2013.

33. Suarez-Rivera, R.; Chertov, M.; Willberg, D.; Green, S.;Keller, J. Understanding Permeability Measurements in Tight Shales Promotes Enhanced Determination of Reservoir Quality. Society of Petroleum Engineers, 2012, Paper SPE 162816-MS presented at CURC 2012, Calgary, Alberta, Oct. 30–Nov. 1.
34. Macquaker, J.H.S. Adams, A.E. Maximizing information from fine-grained sedimentary rocks: An inclusive nomenclature for mudstones: *J. Sedimentary Research*, **2003**, v. 73, p. 735-744.
35. Dehandschutter, B.; Vandycke, S.; Sintubin, M.; Vandenberghe, N.;Wouters, L. Brittle fractures and ductile shear bands in argillaceous sediment: inferences from Oligocene Boom Clay (Belgium): *J. Structural Geology*, 2005, v. 27, p. 1095-1112, doi https://doi.org/10.1016/j.jsg.2004.08.014.
36. Lucier, A.; Zoback, M.; Gupta, N.; Ramakrishnan, T.S. Geomechanical aspects of CO_2 sequestration in a deep saline reservoir in the Ohio River Valley region: *Environmental Geosciences*, **2006**, v. 13, p. 85-103, doi 10.1306/eg.11230505010.
37. Lucier, A.; Zoback, M. Assessing the economic feasibility of regional deep saline aquifer CO_2 injection and storage: a geomechanics-based workflow applied to the Rose Run sandstone in Eastern Ohio, USA. *Int. J. Greenhouse Gas Control*, **2008**, 2(2), 230–247, http://dx.doi.org/10.1016/j.ijggc.2007.12.002.
38. Terra Tek, Fracture Analysis of Core, Farnsworth Unit 13-14 Well, Ochiltree County, Texas. Report TR14-811119, 2014a, Prepared for Chaparral Energy, L.L.C., 69 p.
39. Terra Tek, Fracture Analysis of Core, Farnsworth Unit 32-8 Well, Ochiltree County, Texas. Report TR14-811168, 2014b, Prepared for Chaparral Energy, L.L.C., 69 p.
40. Snee, J.E.L.; Zoback, M.D. 2016, State of stress in Texas: Implications for induced seismicity: *Geophysical Research Letters*, **2016**, v. 43, p. 10208-10214, doi 10.1002/2016GL07097.
41. Terra Tek. Integrated Tight Rock Analysis Whole Core, Farnsworth 13-10A Well, Ochiltree Co., Texas. E-Report TR14-811108, 2014c, Prepared for Chaparraal Energy, L.L.C.
42. Terra Tek. Integrated Tight Rock Analysis Whole Core, Farnsworth 13-14 Well, Ochiltree Co., Texas. E-Report TR14-811119, 2014d, Prepared for Chaparraal Energy, L.L.C.
43. Terra Tek, Integrated Tight Rock Analysis Whole Core, Farnsworth 32-8 Well, Ochiltree Co., Texas. E-Report TR14-811168, 2014e. Prepared for Chaparral Energy, L.L.C.
44. Ballentine, C. J.; R. Burgess; B. Marty. Tracing Fluid origin, transport and interaction in the crust, *in* Noble Gases in Geochemistry and Cosmochemistry: Reviews in Mineralogy and Geochemistry, v. 47, D. Porcelli, C. J. Ballentine, and R. Wieler, eds., Washington, DC, Mineralogical Society of America 2002, p. 539–614.
45. Prinzhofer, A. 2013. Noble Gas in Oil and Gas Accumulations, *in The Noble Gases as Geochemical Tracers, Advances in Isotope Geochemistry*, Burnard, P. (ed.),, Springer-Verlag, New York, 2013, p. 225–247.
46. Xiao, T.; Xu, H.; Moodie, N.; Esser, R.; Jia, W.; Zheng, L.; Rutqvist, J.; McPherson, B. Chemical-mechanical impacts of CO_2 intrusion into heterogeneous caprock. **2020**. *Water Resources Research*, 56, e2020WR027193. doi.org/10.1029/2020WR027193.